Empirical Response Spectral Attenuation Relations for Shallow Crustal Earthquakes

N. A. Abrahamson
Pacific Gas & Electric Co.

W. J. Silva
Pacific Engineering and Analysis

ABSTRACT

Using a database of 655 recordings from 58 earthquakes, empirical response spectral attenuation relations are derived for the average horizontal and vertical component for shallow earthquakes in active tectonic regions. A new feature in this model is the inclusion of a factor to distinguish between ground motions on the hanging wall and footwall of dipping faults. The site response is explicitly allowed to be non-linear with a dependence on the rock peak acceleration level.

INTRODUCTION

Ground motion attenuation relations can be regionalized into three categories: shallow crustal earthquakes in active tectonic regions (*e.g.*, Western North America), shallow crustal events in stable continental regions (*e.g.*, Central and Eastern North America), and subduction zones (*e.g.*, Pacific Northwest and Alaska). In this study, we develop empirical models for the attenuation of response spectral values for both the average horizontal and the vertical components applicable to shallow crustal events in active tectonic regions.

STRONG MOTION DATA SET

The data set used in this study is based on worldwide data which consists of strong ground motions from shallow crustal events in active tectonic regions, excluding subduction events. Events up through the 1994 Northridge earthquake are included. There are 853 recordings from 98 mainshocks and aftershocks with magnitude greater than 4.5 in the full data set. Recordings with unknown or poor estimates of the magnitude, mechanism, distance, or site condition were excluded from the data set used in the regression analysis. This reduced the data set used in the analysis to 655 recordings from 58 earthquakes. The 58 events used in the analysis are listed in Table 1.

Record Processing

All of the records were reprocessed using a common reprocessing procedure. The correction procedure involves 5 steps:

1. interpolation of uncorrected unevenly sampled records to 400 samples/sec;
2. frequency domain low-pass filtering using a causal 5-pole Butterworth filter with the corner frequency selected for each record based on visual examination of the Fourier amplitude spectrum;
3. removing the instrument response;
4. decimating to 100 or 20 samples/sec depending on the low-pass filter corner frequency; and
5. applying a time domain baseline correction procedure and a final high-pass filter.

The baseline correction procedure uses a polynomial in degree 0–10 depending upon the initial integrated displacements. The characteristics of the high-pass filter is that of an overdamped oscillator (Grazier,1979). It is flat about its corner frequency and falls off proportional to frequency on either side. The filter is applied in the time domain twice, forward and reverse, resulting in a zero phase shift processed record. As with the polynomial baseline correction, the high-pass filter parameters are selected based on visual examination of the filtered integrated displacements for a suite of parameter values. The response spectral values are only used in the regression if the frequency is greater than 1.25 times the high-pass corner frequency and less than 1/1.25 times the low-pass corner frequency. This ensures that the filter will not have a significant effect on the response spectral values used in the regression. This requirement produces a data set that varies as a function of period. The number of recordings in the final data set is shown in Figure 1 as a function of period.

Site Classification

The site classification is based on the Geomatrix site class that is given in Table 2. In this study, we have combined Geomatrix site class C and D into a single deep soil site category. The Geomatrix A and B classes (rock and shallow soil) were also combined into a single "rock" site category.

TABLE 1
Earthquakes Used in the Regression Analysis

Event #	Earthquake	Date & Time	Mag
6	Imperial Valley	1940 0519 0437	7.0
12	Kern County	1952 0721 1153	7.4
20	San Francisco	1957 0322 1944	5.3
25	Parkfield	1966 0628 0426	6.1
28	Borrego Mtn	1968 0409 0230	6.8
29	Lytle Creek	1970 0912 1430	5.4
30	San Fernando	1971 0209 1400	6.6
31	Point Mugu	1973 0221 1445	5.8
32	Hollister	1974 1128 2301	5.2
34	Oroville	1975 0801 2020	6.0
35	Oroville	1975 0802 2022	5.0
36	Oroville	1975 0802 2059	4.4
37	Oroville	1975 0808 0700	4.7
38	Friuli, Italy	1976 0506 2000	6.5
39	Gazli, USSR	1976 0517	6.8
41	Friuli, Italy	1976 0915 0315	6.1
42	Santa Barbara	1978 0813	6.0
43	Tabas, Iran	1978 0916	7.4
44	Coyote Lake	1979 0806 1705	5.7
45	Imperial Valley	1979 1015 2316	6.5
46	Imperial Valley	1979 1015 2319	5.2
47	Imperial Valley	1979 1016 0658	5.5
48	Livermore	1980 0124 1900	5.8
49	Livermore	1980 0127 0233	5.4
50	Anza	1980 0225 1047	4.9
57	Mammoth Lakes AS	1980 0527 1901	4.9
58	Mammoth Lakes AS	1980 0531 1516	4.9
59	Victoria, Mexico	1980 0609 0328	6.4
60	Mammoth Lakes AS	1980 0611 0441	5.0
62	Taiwan (SMART #5)	1981 0129	5.7
63	Westmorland	1981 0426 1209	5.8
66	Coalinga	1983 0502 2342	6.4
67	Coalinga	1983 0509 0249	5.0
68	Coalinga	1983 0611 0309	5.3
69	Coalinga	1983 0709 0740	5.2
70	Coalinga	1983 0722 0239	5.8
71	Coalinga	1983 0722 0343	4.9
72	Coalinga	1983 0725 2231	5.2
74	Coalinga	1983 0909 0916	5.3
76	Morgan Hill	1984 0424 2115	6.2
77	Bishop (Rnd Val)	1984 1123 1912	5.8
79	Nahanni, Canada	1985 1223	6.8
80	Hollister	1986 0126 1920	5.4
82	Taiwan (SMART #40)	1986 0520	6.4
83	N. Palm Springs	1986 0708 0920	6.0
84	Chalfant Valley	1986 0720 1429	5.9
85	Chalfant Valley	1986 0721 1442	6.2
86	Chalfant Valley	1986 0721 1451	5.6
87	Chalfant Valley	1986 0731 0722	5.8
89	Whittier Narrows	1987 1001 1442	6.0
90	Whittier Narrows	1987 1004 1059	5.3
91	Superstitn Hills(A)	1987 1124 0514	6.3
92	Superstitn Hills(B)	1987 1124 1316	6.7
93	Spitak, Armenia	1988 1207	6.8
94	Loma Prieta	1989 1018 0005	6.9
96	Cape Mendocino	1992 0425 1806	7.1
97	Landers	1992 0628 1158	7.3
98	Northridge	1994 0117 1231	6.7

TABLE 1 (Continued)
Earthquakes Used in the Regression Analysis

TABLE 2
Site Classification (from Geomatrix)

A	Rock (Vs > 600 m/s) or very thin soil (< 5m) over rock
B	Shallow Soil Soil 5-20 m thick over rock
C	Deep Soil in Narrow Canyon Soil > 20 m thick Canyon < 2 km wide
D	Deep Soil in Broad Canyon Soil > 20 m thick Canyon >2 km wide
E	Soft Soil (Vs < 150 m/s)

Although the site classification listed in Table 2 has quantitative values, for most of the sites, such quantitative information is not available, so the sites are classified subjectively using the criteria listed in Table 2 as a guide rather than a strict classification scheme.

Distance Definition

Several different distance definitions have been used for developing attenuation relations. In this study, we have used the closest distance to the rupture plane, r_{rup}. This is the same distance as used by Idriss (1991) and Sadigh *et al.* (1993). The distribution of the data in terms of magnitude and distance space is shown for four periods (T = 5.0, 1.0, 0.2, and 0.075 seconds) in Figures 2 and 3 for the horizontal and vertical components, respectively.

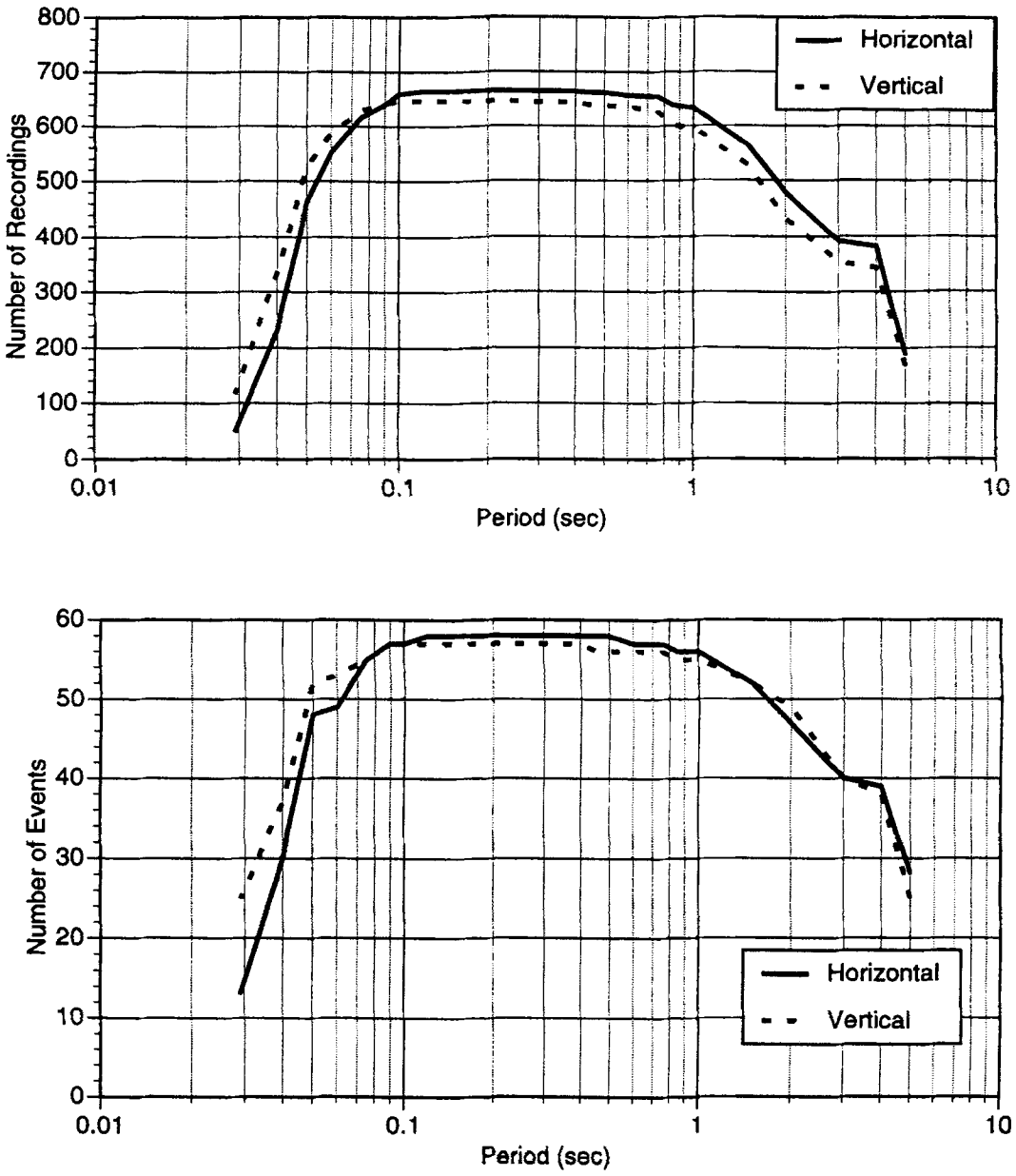

▲ **Figure 1.** Period dependence of the number of events (lower) and number of recordings (upper) used in the regression analysis.

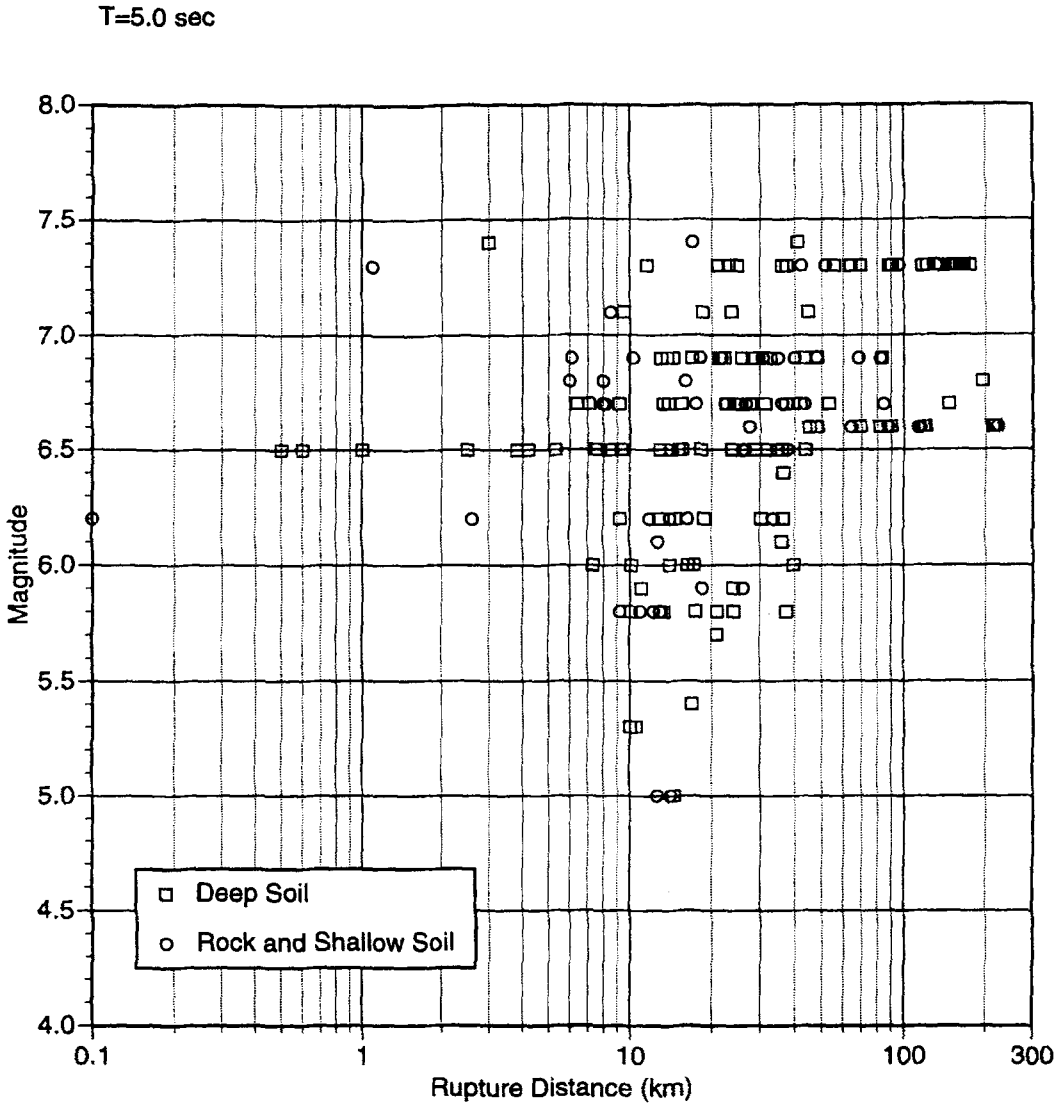

▲ **Figure 2a.** Distribution of data for 5.0 seconds period for the horizontal component.

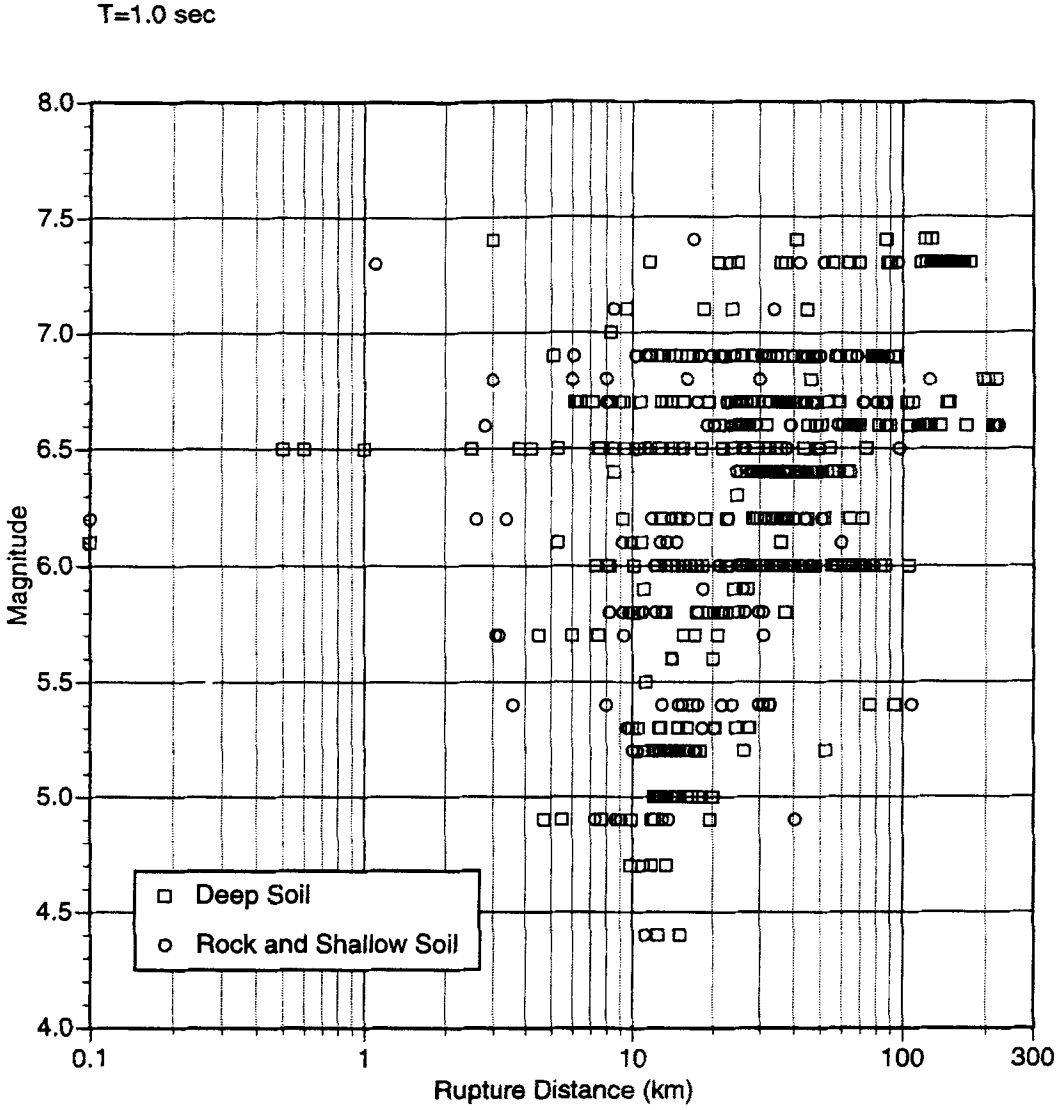

▲ **Figure 2b.** Distribution of data for 1.0 second period for the horizontal component.

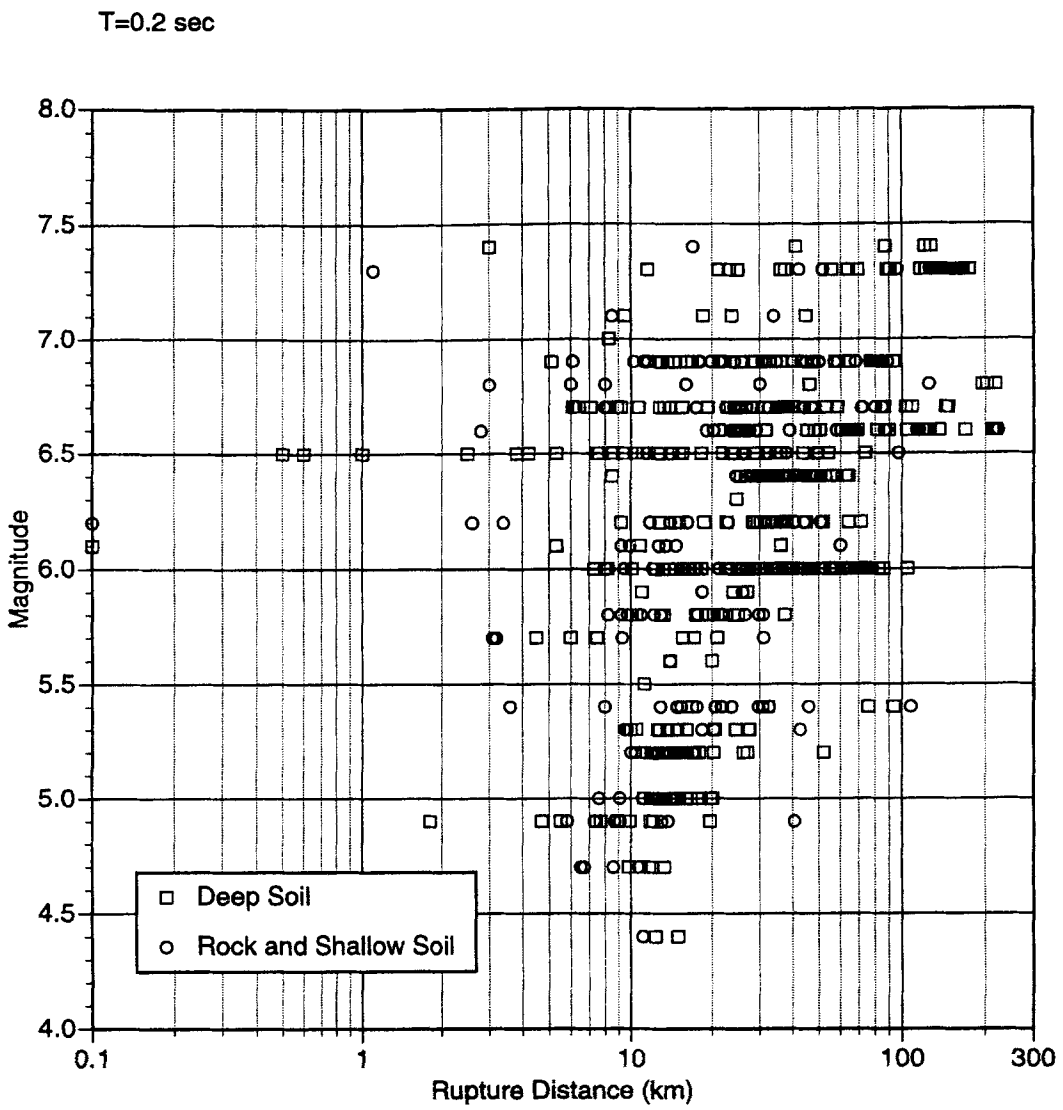

▲ **Figure 2c.** Distribution of data for 0.2 second period for the horizontal component.

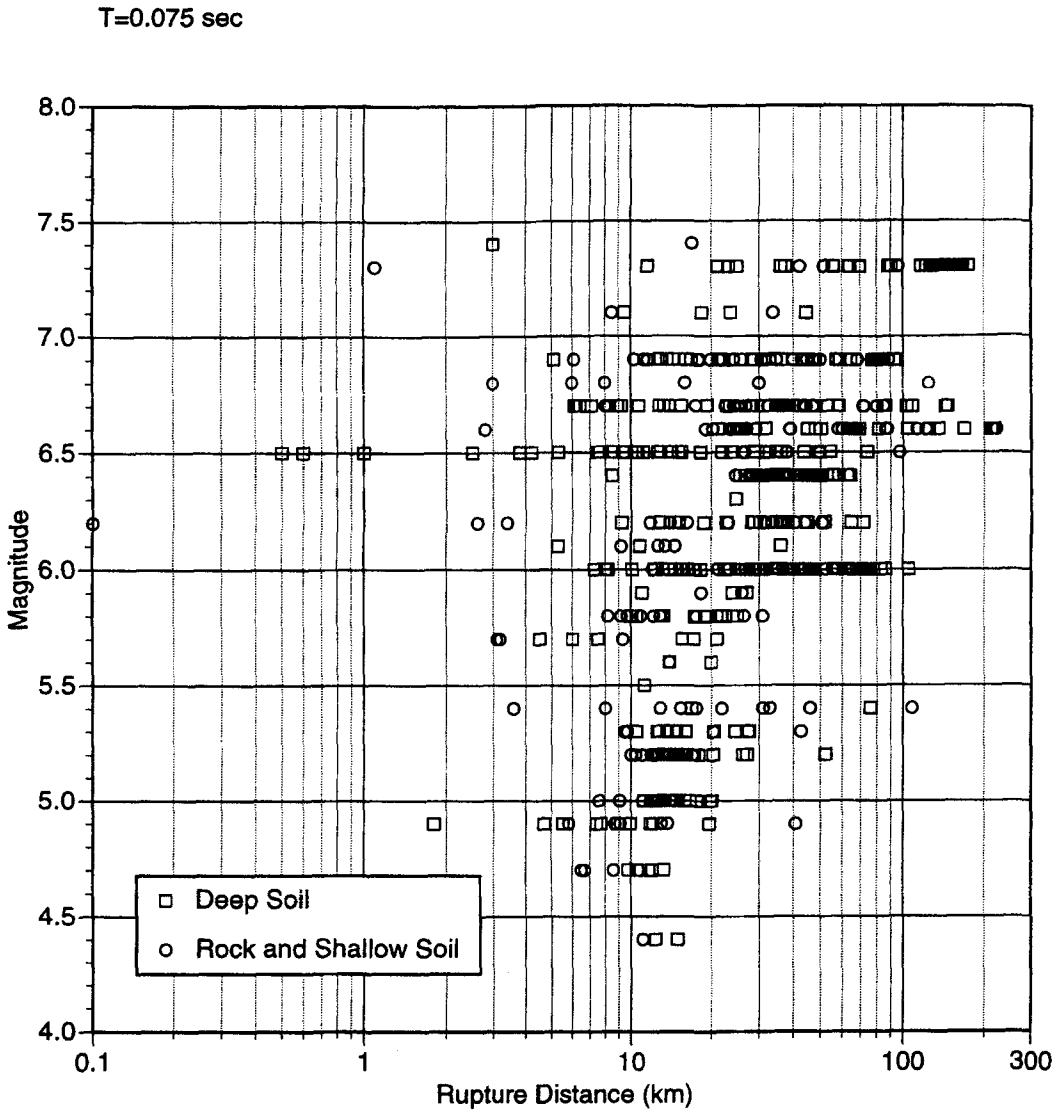

▲ **Figure 2d.** Distribution of data for 0.075 second period for the horizontal component.

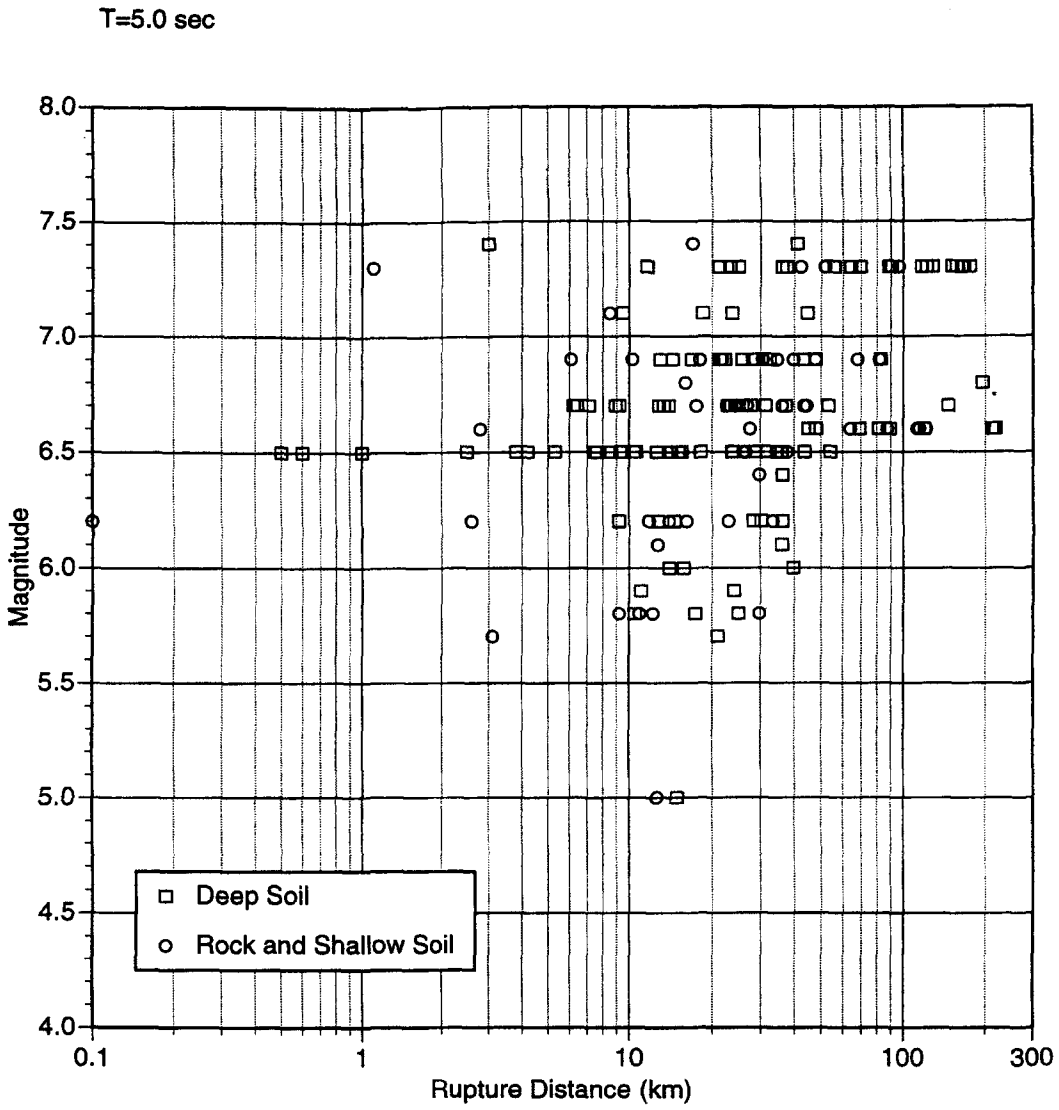

▲ **Figure 3a.** Distribution of data for 5.0 seconds period for the vertical component.

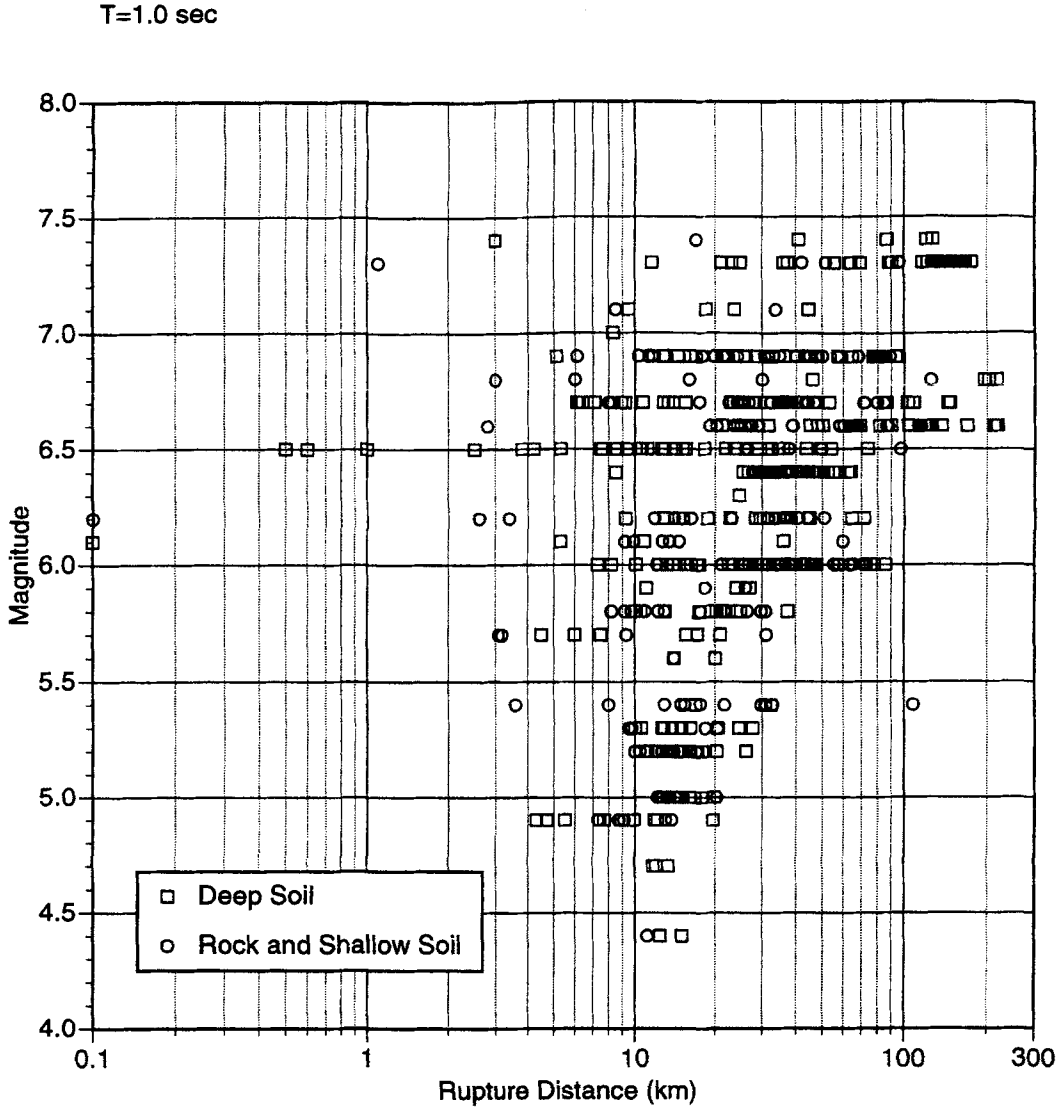

▲ **Figure 3b**. Distribution of data for 1.0 second period for the vertical component.

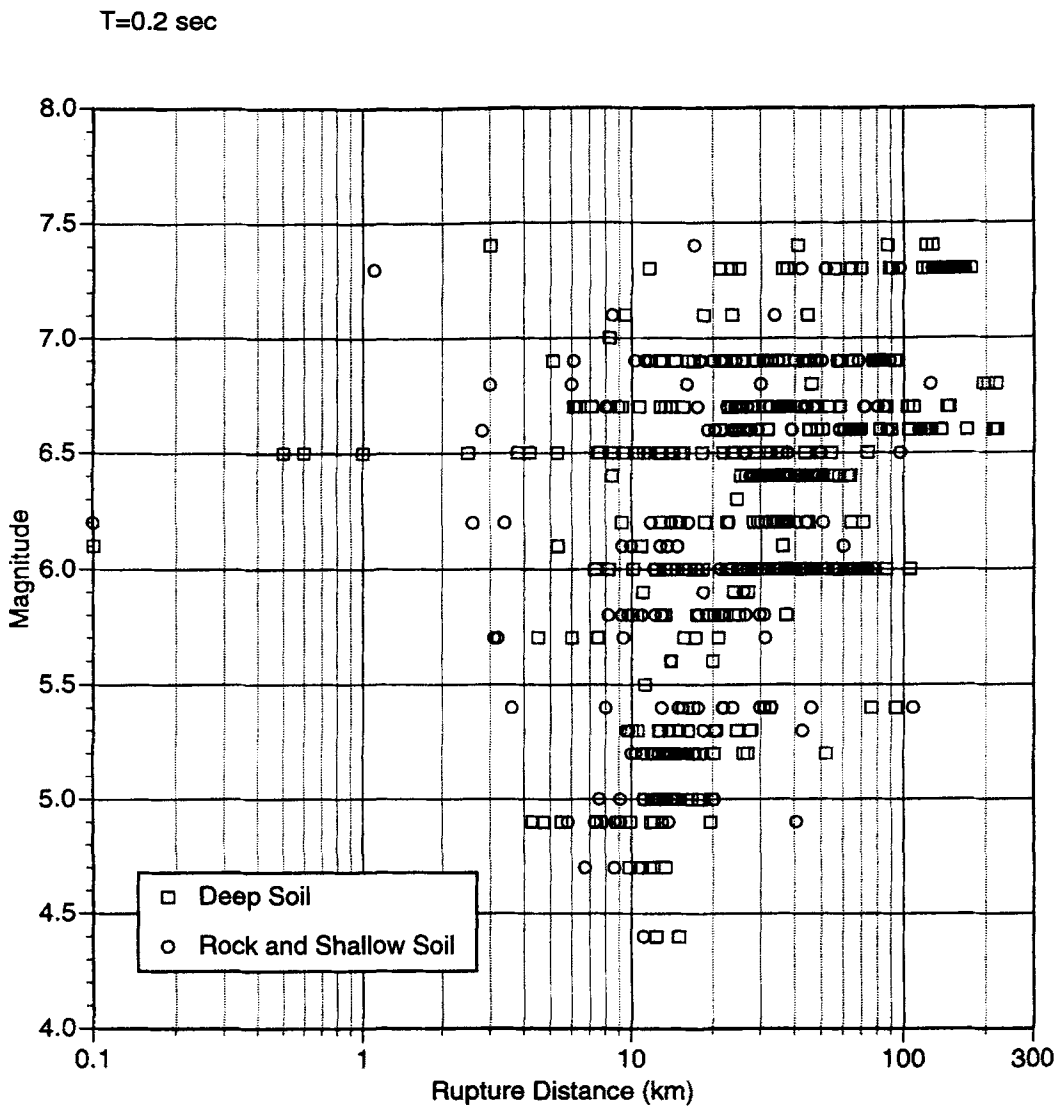

▲ **Figure 3c.** Distribution of data for 0.2 second period for the vertical component.

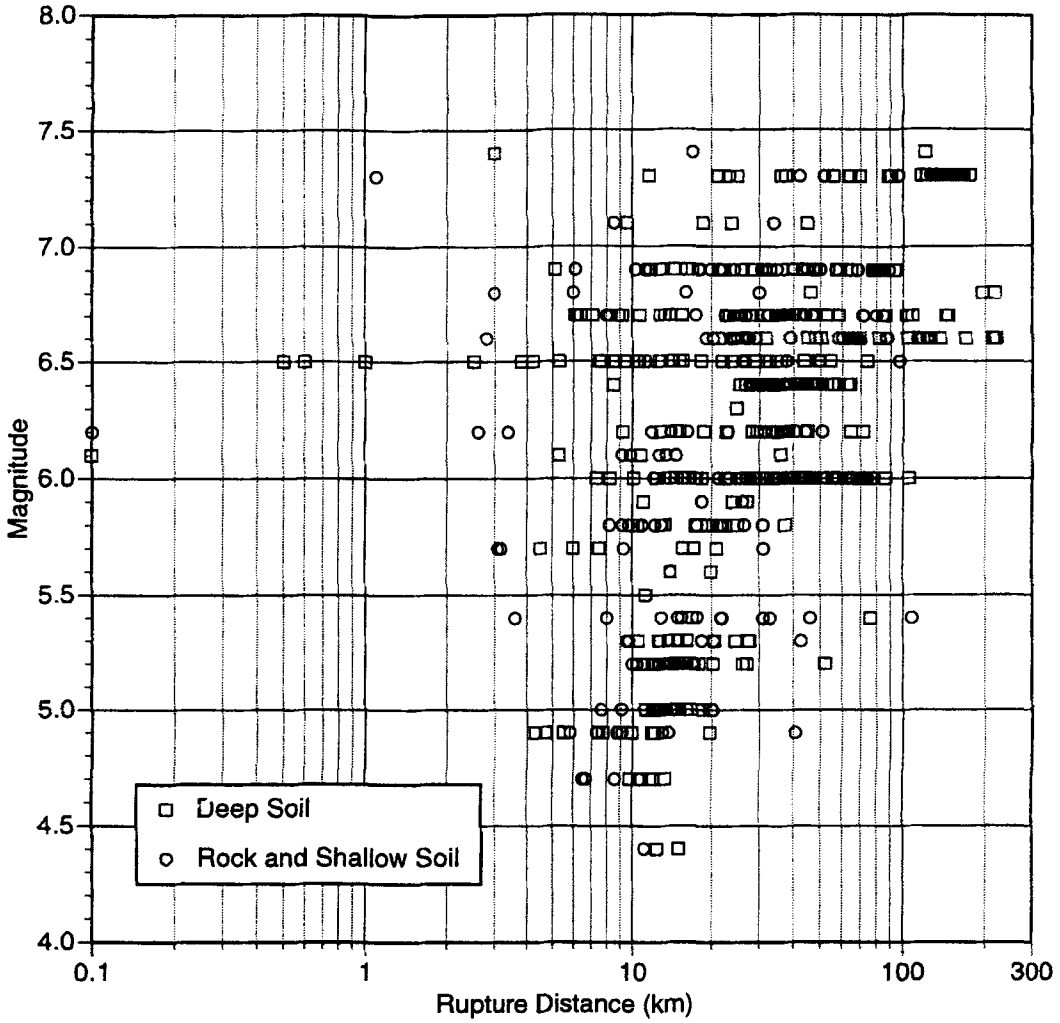

▲ **Figure 3d.** Distribution of data for 0.075 second period for the vertical component.

DEVELOPMENT OF ATTENUATION RELATIONS

Regression Method

We use a random effects model for the regression analysis. The random effects model is a maximum likelihood method that accounts for correlations in the data recorded by a single earthquake. For example, if an earthquake has a higher than average stress drop, then the ground motions at all sites from this event are expected to be higher than average. We use the procedure described by Abrahamson and Youngs (1992) to apply the random effect model. In a standard fixed effects regression, the model can be written as

$$Y_k = f(M_k, r_k) + \varepsilon_k \tag{1}$$

where Y_k is the ground motion, M_k is the magnitude and r_k is the distance for the kth data point. The ε_k term is assumed to be normally distributed with mean zero. The standard error of the ε_k values gives the standard error of the model.

In contrast, the random effects model can be written as

$$Y_{ij} = f(M_i, r_{ij}) + \varepsilon_{ij} + \eta_i \tag{2}$$

where Y_{ij} is the ground motion for the jth recordings from the ith earthquake, M_i is magnitude of the ith earthquake, and r_{ij} is the distance for the jth recordings from the ith earthquake. There are two stochastic terms in the model. Both ε_{ij} and η_i are assumed to be normally distributed with mean zero. The random effects model uses the maximum likelihood method to partition the residual for each recording into the ε_{ij} and η_i terms. There are two parts to the standard error for the model: an inter-event term, τ, which is the standard error of the η_i and intra-event term, σ, which is the

standard error of the ε_{ij}. The total standard error of the model is

$$\sqrt{\sigma^2 + \tau^2}\ .$$

The Joyner and Boore (1981) two-step method also accounts for the correlation in the data from a single earthquake by explicitly estimating an event term for each event in the first step. In their model, the random terms, η_i, are replaced by fixed effects terms (coefficients of the model). The random effects model differs from the two-step method described by Joyner and Boore (1981) in that for events with only a few recordings, part of the mean event term may be due to random variations of the data (intra-event variations) and poor sampling of the event. As described by Abrahamson and Youngs (1992), for poorly sampled events, the random effects method estimates how much of the event term is likely to be due to random sampling of the intra-event distribution and how much is likely to be due to systematic differences between the event and the average. If all of the events have a large number of recordings, then the two-step method and the random effects method become equivalent.

Regression Model

In developing the functional form of the regression equation, we combined features of the regression equations that have been used in previous studies. The general functional form that we employ is given by:

$$\ln Sa(g) = f_1(M, r_{rup}) + Ff_3(M) + HWf_4(M, r_{rup}) + Sf_5(\widehat{\text{pga}}_{\text{rock}}) \quad (3)$$

where $Sa(g)$ is the spectral acceleration in g, M is moment magnitude, r_{rup} is the closest distance to the rupture plane in km, F is the fault type (1 for reverse, 0.5 for reverse/oblique, and 0 otherwise), HW is the dummy variable for hanging wall sites (1 for sites over the hanging wall, 0 otherwise), and S is a dummy variable for the site class (0 for rock or shallow soil, 1 for deep soil). For the horizontal component, the geometric mean of the two horizontals is used.

The function $f_1(M, r_{rup})$ is the basic functional form of the attenuation for strike-slip events recorded at rock sites. For $f_1(M, r_{rup})$, we have used the following form:

$$\text{for } M \le c_1$$
$$f_1(M, r_{rup}) = a_1 + a_2(M - c_1) + a_{12}(8.5 - M)^n + \left[a_3 + a_{13}(M - c_1)\right]\ln R$$
$$\text{for } M > c_1 \quad (4)$$
$$f_1(M, r_{rup}) = a_1 + a_4(M - c_1) + a_{12}(8.5 - M)^n + \left[a_3 + a_{13}(M - c_1)\right]\ln R$$

where

$$R = \sqrt{r_{rup}^2 + c_4^2} \quad (5)$$

This form is a composite of several previous studies. The slope of the log distance term is magnitude dependent as was used by Idriss (1991). The Idriss model differs from our model in that it uses exponential models for the magnitude dependence of the slope whereas we have used a linear dependence. The saturation of high frequency ground motion at short distances is accommodated by the magnitude dependent slope.

For long periods, a linear magnitude dependence is not adequate. Most recent studies have found that higher order terms are needed. Boore *et al.* (1993) include a quadratic term; Campbell (1993) includes a hyperbolic arctangent term, Idriss (1991) includes an exponential magnitude term, and Sadigh *et al.* (1993) includes a higher order polynomial term. These different models give similar models when fit to the same data. We have adopted the functional form used by Sadigh *et al.* (1993).

For the distance term inside the log, we have used the

$$\sqrt{r_{rup}^2 + c_4^2}$$

model similar to that used by Boore *et al.* (1993). In the Boore *et al.* (1993) model, the c_4 term can be interpreted as a fictitious depth. In our model, however, we are using the rupture distance (which can include depth for dipping faults and for fault that do not reach the surface), so the interpretation of c_4 as a depth term is not clear. Nevertheless, we have adopted the

$$\sqrt{r_{rup}^2 + c_4^2}$$

model because it yields a marginally better fit to the data at short distances.

Style-of-Faulting Factor

The distinction between ground motions from strike-slip and reverse faults has become common in recent attenuation relations (*e.g.*, Idriss, 1991; Sadigh *et al.*, 1993; Boore *et al.*, 1997; Campbell and Bozorgnia, 1994). The difference in ground motion between reverse and strike-slip events is called the style-of-faulting factor. Most attenuation relations have considered a constant style-of-faulting factor that applies to all magnitudes, distances, and periods. Sadigh *et al.* (1993) and Campbell and Bozorgnia (1994) included a magnitude and distance dependence of the style-of-faulting for peak acceleration. Boore *et al.* (1997) include a period dependence to the style-of-faulting factor.

In this study, we have used a functional form that allows for a magnitude and period dependence of the style-of-faulting factor:

$$f_3(M) = \begin{cases} a_5 & \text{for } M \le 5.8 \\ a_5 + \dfrac{(a_6 - a_5)}{c_1 - 5.8} & \text{for } 5.8 < M < c_1 \\ a_6 & \text{for } M \ge c_1 \end{cases} \quad (6)$$

Hanging Wall Effect

We also followed the approach used by Somerville and Abrahamson (1995) to model the differences in the motion on the hanging wall and foot wall of dipping faults. In this previous study, a comparison was made between the ground motions for sites on the hanging wall with those on the foot wall and with those off the ends of the fault rupture. A significant systematic increase in ground motions was found for sites over the hanging wall, but the decrease in ground motion for sites on the foot wall was not as systematic. As a result, the ground motion for dipping faults was separated into two categories: sites on the hanging wall side of the rupture and within the edge of the rupture, and sites on the foot wall side or off the end of the rupture. The hanging wall effect is considered to be primarily a geometric effect that results from the distance definition used in this study. (The distance measure used by Boore *et al.*, 1993 implicitly accounts for the difference in the ground motion over the hanging wall and footwall.) The magnitude and distance dependence of the functional form, $f_4(M, r_{rup})$, for the hanging wall effect is taken from Somerville and Abrahamson (1995) and is modeled as separable in magnitude and distance so that

$$f_4(M, r_{rup}) = f_{HW}(M)\, f_{HW}(r_{rup}) \quad (7)$$

where

$$f_{HW}(M) = \begin{cases} 0 & \text{for } M \le 5.5 \\ M - 5.5 & \text{for } 5.5 < M < 6.5 \\ 1 & \text{for } M \ge 6.5 \end{cases} \quad (8)$$

and

$$f_{HW}(r_{rup}) = \begin{cases} 0 & \text{for } r_{rup} < 4 \\ a_9 \dfrac{r_{rup} - 4}{4} & \text{for } 4 < r_{rup} < 8 \\ a_9 & \text{for } 8 < r_{rup} < 18 \\ a_9 \left(1 - \dfrac{r_{rup} - 18}{7}\right) & \text{for } 18 < r_{rup} < 24 \\ 0 & \text{for } r_{rup} > 25 \end{cases} \quad (9)$$

Site Response

A key aspect is the use of a functional form that accommodates non-linear soil response. We followed the approach used by Youngs (1993) in which the soil amplification is a function of the expected peak acceleration on rock. This approach allows a single regression for both soil and rock while preserving the differences between soil and rock attenuation.

The non-linear soil response is modeled by

$$f_5\left(\widehat{\mathrm{PGA}}_{\mathrm{rock}}\right) = a_{10} + a_{11} \ln\left(\widehat{\mathrm{PGA}}_{\mathrm{rock}} + c_5\right) \quad (10)$$

where $\widehat{\mathrm{PGA}}_{\mathrm{rock}}$ is the expected peak acceleration on rock in g (as predicted by the median attenuation relation with S = 0). A similar functional form was proposed by Youngs (1993); the only difference here is the addition of the c_5 term.

Standard Error

Several recent attenuation studies have found that the standard error is dependent on the magnitude of the earthquake (Sadigh, 1993; Idriss, 1991; Campbell, 1993) or is dependent on the level of shaking (Campbell and Bozorgnia, 1994). This issue is discussed at length in Youngs *et al* (1995).

In this study, both the inter-event (τ) and intra-event (σ) standard errors are allowed to be magnitude dependent and are modeled as follows:

$$\sigma(M) = \begin{cases} b_1 & \text{for } M \le 5.0 \\ b_1 - b_2(M - 5) & \text{for } 5.0 < M < 7.0 \\ b_1 - 2b_2 & \text{for } M \ge 7.0 \end{cases} \quad (11)$$

and

$$\tau(M) = \begin{cases} b_3 & \text{for } M \le 5.0 \\ b_3 - b_4(M - 5) & \text{for } 5.0 < M < 7.0 \\ b_3 - 2b_4 & \text{for } M \ge 7.0 \end{cases} \quad (12)$$

The magnitude dependence of the standard error is estimated using the random effects model which avoids underestimating the standard error for large magnitude events due to the fewer number of events (as compared to small and moderate magnitude events).

The total standard error is then computed by adding the variance of the two error terms. The total standard error was then smoothed and fit to the form

$$\sigma_{\mathrm{total}}(M) = \begin{cases} b_5 & \text{for } M \le 5.0 \\ b_5 - b_6(M - 5) & \text{for } 5.0 < M < 7.0 \\ b_5 - 2b_6 & \text{for } M \ge 7.0 \end{cases} \quad (13)$$

Sa vs Sa/pga

In many previous studies for response spectral attenuation, the regression has been separated into two steps: a regression for the peak acceleration and a regression for the normalized spectral shape, Sa/pga. An advantage of this approach is that the normalized spectral values are less variable than the spectral accelerations. Therefore, the higher order terms in the magnitude dependence can be estimated with less uncertainty. One assumption that is usually made when using nomalized spectral values is that the magnitude saturation term (term inside the log) for spectral acceleration at all periods is the same as for peak acceleration. This assumption greatly simplifies the functional form of the normalized spectral shape. This assumption is the biggest potential drawback of using the normalized spectra approach. The Boore *et al.* (1993) model shows that the c_4 term is period dependent. If a period dependent c_4 term is used, then the resulting regression model becomes so complex that you have lost much of the advantage of using normalized spectral shapes.

We have dealt with this issue by fitting the Sa values directly (not normalized shapes) but restricting some of the coefficients to be independent of period. Reducing the number of coefficients that are period dependent helps to keep the response spectral values smoothly varying functions of distance, magnitude, and period without introducing bumps into the spectra.

Regression Results—Horizontal Component

The regression is computed using multiple steps. The multiple steps are used to constrain the resulting model to be a smooth function of period for all magnitudes, distances, mechanisms, and site conditions. Following each step, the period dependence of the uncorrelated coefficients was smoothed using piecewise continuous linear fits on the log period axis. For highly correlated coefficients, one coefficient was smoothed and then the other coefficients were re-estimated.

In the first step, the peak acceleration is fit to Eq. (3) with a_{12} set to zero. The values of a_{13}, a_2, and a_4 are then fixed for the subsequent spectral values regression. In the second step, the spectral acceleration values are fit to Eq. (3). In the third step, the c_4 term was held fixed, and all of the other model parameters were estimated. In the fourth step, the all coefficients except a_{10} and a_1 were fixed and new a_1 and a_{10} values were estimated. In the fifth step, all coefficients except a_1 were held fixed and new a_1 values were estimated. The final smoothing on a_1 forces the model to produce smooth spectra for spectral velocity and displacement as well as for spectral acceleration. The final coefficients are listed in Table 3.

We then evaluated the magnitude dependence of the standard errors for the final fit. The raw estimates of the inter-event and intra-event standard errors were combined to estimate the total standard error. The standard errors were smoothed by hand to produce the final model for the standard error (Table 4).

The residuals of the model as shown in Figures 4 and 5 for periods of 1.0, 0.3, and 0.1 seconds. Since we are using the random effects model, there are two parts to the residual: an intra-event term and an inter-event term. These residuals are shown separately in Figures 4 and 5.

Regression Results—Vertical Component

The model for the vertical component was developed using the same functional form and multiple step procedure as for the horizontal component. The final smoothed model coefficients are listed in Table 5. The smoothed standard errors are listed in Table 6. The residuals for periods of 1.0, 0.3, and 0.1 sec are plotted by r_{rup} and M in Figures 6 and 7, respectively.

Model Predictions

Examples of the median ground motions for strike-slip events are shown in Figures 8 and 9 for the horizontal component and in Figures 10 and 11 for the vertical component.

DISCUSSION OF THE EMPIRICAL MODEL

There are several limitations of the empirical model developed in this study that should be considered in the application of the model to engineering projects.

The way the data set was constructed produces a data set that is biased to the larger motions. Ground motions that are larger than average have a higher likelihood of being above the noise level than ground motions from data that are smaller than average. Since the usable bandwidth of each recording was evaluated separately, rather than finding a single usable bandwidth for all of the data, we will likely have more larger than average recordings in the data set for the periods not completely sampled (< 0.1 sec and > 2 sec). By not using a cutoff to the first non-triggered instrument, we also tend to have ground motions biased to the larger values. We decided that it was preferable to have some biased data than to have no data for the high frequencies and long periods, so we accepted this bias.

The site response factor (f_5 in Eq. 10) is dependent on only the expected peak acceleration on rock. It does not include a magnitude dependence to the site effect. While we consider this model to be an improvement over models that only consider a constant scale factor for the site effect at each period, this model does not include all of the effects that may be found in site specific studies based on analytical models of the site effect.

The style-of-faulting factor (f_3 in Eq. 6) has a strong magnitude dependence. For rock sites, the effect is about 30% for large magnitude events but almost a factor of 2 for small (M < 5.8) magnitude events. This strong magnitude dependence is driven by the Coalinga aftershock sequence which represents 8 of the 11 reverse and reverse/oblique events with magnitude less than 5.8. This sequence produced larger than average high frequency motion which lead to a large style-of-faulting factor for small magnitude events. The events in the sequence were treated as uncorrelated in the random effects model. If a sequence random effect was

TABLE 3.
Coefficients for the Average Horizontal Component

Period	c_4	a_1	a_2	a_3	a_4	a_5	a_6	a_9	a_{10}	a_{11}	a_{12}	a_{13}	c_1	c_5	n
5.00	3.50	−1.460	0.512	−0.7250	−0.144	0.400	−0.200	0.000	0.664	0.040	−0.2150	0.17	6.4	0.03	2
4.00	3.50	−1.130	0.512	−0.7250	−0.144	0.400	−0.200	0.039	0.640	0.040	−0.1956	0.17	6.4	0.03	2
3.00	3.50	−0.690	0.512	−0.7250	−0.144	0.400	−0.156	0.089	0.630	0.040	−0.1726	0.17	6.4	0.03	2
2.00	3.50	−0.150	0.512	−0.7250	−0.144	0.400	−0.094	0.160	0.610	0.040	−0.1400	0.17	6.4	0.03	2
1.50	3.55	0.260	0.512	−0.7721	−0.144	0.438	−0.049	0.210	0.600	0.040	−0.1200	0.17	6.4	0.03	2
1.00	3.70	0.828	0.512	−0.8383	−0.144	0.490	0.013	0.281	0.423	0.000	−0.1020	0.17	6.4	0.03	2
0.85	3.81	1.020	0.512	−0.8648	−0.144	0.512	0.038	0.309	0.370	−0.028	−0.0927	0.17	6.4	0.03	2
0.75	3.90	1.160	0.512	−0.8852	−0.144	0.528	0.057	0.331	0.320	−0.050	−0.0862	0.17	6.4	0.03	2
0.60	4.12	1.428	0.512	−0.9218	−0.144	0.557	0.091	0.370	0.194	−0.089	−0.0740	0.17	6.4	0.03	2
0.50	4.30	1.615	0.512	−0.9515	−0.144	0.581	0.119	0.370	0.085	−0.121	−0.0635	0.17	6.4	0.03	2
0.46	4.38	1.717	0.512	−0.9652	−0.144	0.592	0.132	0.370	0.020	−0.136	−0.0594	0.17	6.4	0.03	2
0.40	4.52	1.860	0.512	−0.9880	−0.144	0.610	0.154	0.370	−0.065	−0.160	−0.0518	0.17	6.4	0.03	2
0.36	4.62	1.955	0.512	−1.0052	−0.144	0.610	0.170	0.370	−0.123	−0.173	−0.0460	0.17	6.4	0.03	2
0.30	4.80	2.114	0.512	−1.0350	−0.144	0.610	0.198	0.370	−0.219	−0.195	−0.0360	0.17	6.4	0.03	2
0.24	4.97	2.293	0.512	−1.0790	−0.144	0.610	0.232	0.370	−0.350	−0.223	−0.0238	0.17	6.4	0.03	2
0.20	5.10	2.406	0.512	−1.1150	−0.144	0.610	0.260	0.370	−0.445	−0.245	−0.0138	0.17	6.4	0.03	2
0.17	5.19	2.430	0.512	−1.1350	−0.144	0.610	0.260	0.370	−0.522	−0.265	−0.0040	0.17	6.4	0.03	2
0.15	5.27	2.407	0.512	−1.1450	−0.144	0.610	0.260	0.370	−0.577	−0.280	0.0050	0.17	6.4	0.03	2
0.12	5.39	2.272	0.512	−1.1450	−0.144	0.610	0.260	0.370	−0.591	−0.280	0.0180	0.17	6.4	0.03	2
0.10	5.50	2.160	0.512	−1.1450	−0.144	0.610	0.260	0.370	−0.598	−0.280	0.0280	0.17	6.4	0.03	2
0.09	5.54	2.100	0.512	−1.1450	−0.144	0.610	0.260	0.370	−0.609	−0.280	0.0300	0.17	6.4	0.03	2
0.075	5.58	2.037	0.512	−1.1450	−0.144	0.610	0.260	0.370	−0.628	−0.280	0.0300	0.17	6.4	0.03	2
0.06	5.60	1.940	0.512	−1.1450	−0.144	0.610	0.260	0.370	−0.665	−0.280	0.0300	0.17	6.4	0.03	2
0.05	5.60	1.870	0.512	−1.1450	−0.144	0.610	0.260	0.370	−0.620	−0.267	0.0280	0.17	6.4	0.03	2
0.04	5.60	1.780	0.512	−1.1450	−0.144	0.610	0.260	0.370	−0.555	−0.251	0.0245	0.17	6.4	0.03	2
0.03	5.60	1.690	0.512	−1.1450	−0.144	0.610	0.260	0.370	−0.470	−0.230	0.0143	0.17	6.4	0.03	2
0.02	5.60	1.640	0.512	−1.1450	−0.144	0.610	0.260	0.370	−0.417	−0.230	0.0000	0.17	6.4	0.03	2
0.01	5.60	1.640	0.512	−1.1450	−0.144	0.610	0.260	0.370	−0.417	−0.230	0.0000	0.17	6.4	0.03	2

TABLE 4.
Coefficients for Standard Errors for the Average Horizontal Component

Period	b_5	b_6
5.00	0.89	0.087
4.00	0.88	0.092
3.00	0.87	0.097
2.00	0.85	0.105
1.50	0.84	0.110
1.00	0.83	0.118
0.85	0.82	0.121
0.75	0.81	0.123
0.60	0.81	0.127
0.50	0.80	0.130
0.46	0.80	0.132
0.40	0.79	0.135
0.36	0.79	0.135
0.30	0.78	0.135
0.24	0.77	0.135
0.20	0.77	0.135
0.17	0.76	0.135
0.15	0.75	0.135
0.12	0.75	0.135
0.10	0.74	0.135
0.09	0.74	0.135
0.075	0.73	0.135
0.06	0.72	0.135
0.05	0.71	0.135
0.04	0.71	0.135
0.03	0.70	0.135
0.02	0.70	0.135
0.01	0.70	0.135

included in addition to (or in place of) the event random effect, then this large magnitude dependence of the style-of-faulting factor may be reduced.

Finally, the rock relation is based on a combination of the rock (class A) and shallow soil (class B) sites. Although the B class includes soils up to 20 m thick (Table 2), most of the sites are for much shallower soils. Therefore, we expect significant site response differences for predicting ground motions for a 20 m thick soil site than are predicted by our rock relation. ■

ACKNOWLEDGMENTS

This study was funded by Brookhaven National Laboratory. Strong motion data used in this study were provided by the California Division of Mines and Geology Strong Motion Instrumentation Program; the U.S. Geological Survey; Southern California Earthquake Center; Southern California Edision; Los Angeles Dept. Water and Power; Institue of Earth Sciences Academia Sinica, Taiwan.

REFERENCES

Abrahamson, N. A. and R. R. Youngs (1992). A stable algorithm for regression analyses using the random effects model, *Bull. Seism. Soc. Am.*, **82**, 505–510.

Boore, D. M., W. B. Joyner, and T. Fumal (1993). Estimation of response spectra and peak accelerations from Western North American earthquakes: an interim report, *U.S. Geological Survey, Open File Report 93-509.*

Boore, D. M., W. B. Joyner, and T. Fumal (1997). Equations for estimating horizontal response spectra and peak acceleration in western North American earthquakes, *Seism. Res. Lett.*, **68**, 128–153.

Campbell, K. W. (1993). Empirical prediction of near-source ground motion from large earthquakes, Proc. International Workshop on Earthquake Hazard and Large Dams in the Himalaya, January 15–16, 1993, New Delhi, India.

Campbell, K. W. and Y. Bozorgnia (1994). Near-source attenuation of peak horizontal acceleration from worldwide accelerograms recorded from 1957 to 1993, *Proc. Fifth National Conf. Earthquake Eng., III,* 283–192.

Grazier, V. M. (1979). Determination of the true ground displacement by using strong motion records, *Phys. Solid Earth, Izv. Acad. Sc. USSR,* English ed published by AGU, **15**:(12) 875–885.

Idriss, I. M. (1991). Selection of Earthquake ground motions at rock sites, Report prepared for the Structures Div., Building and Fire Research Lab., NIST.

Sadigh, K, C-Y Chang, N. A. Abrahamson, S. J. Chiou, and M. Power, (1993). Specification of long period motions: updated attenuation relations for rock site conditions and adjustment factors for near-fault effects, Proc. ATC 17-1, 59–70.

Somerville, P. G. and N. A. Abrahamson (1995). Prediction of ground motions for thrust earthquakes, Report to Calif. Strong Motion Instrumentation Program.

Youngs, R. R. (1993). Soil amplification and vertical to horizontal ratios for analysis of strong motion data from active tectonic regions, Appendix 2C in *Guidelines for Determing Design Basis Ground Motions, Vol 2:* appendices for ground motion estimation, TR-102293.

Youngs, R. R., N. A. Abrahamson, F. Makdisi, and K. Sadigh (1995). Magnitude dependent dispersion in peak ground acceleration, *Bull. Seism. Soc. Am.*, **85**, 1,161–1,176.

Pacific Gas & Electric Co., Geosciences Department
P.O. Box 770000, Mail Code N4C
San Francisco, CA 94177
(N.A.A.)

Pacific Engineering and Analysis
311 Pomona Avenue
El Cerrito, CA 94530
e-mail: pacific@crl.com
(W.J.S.)

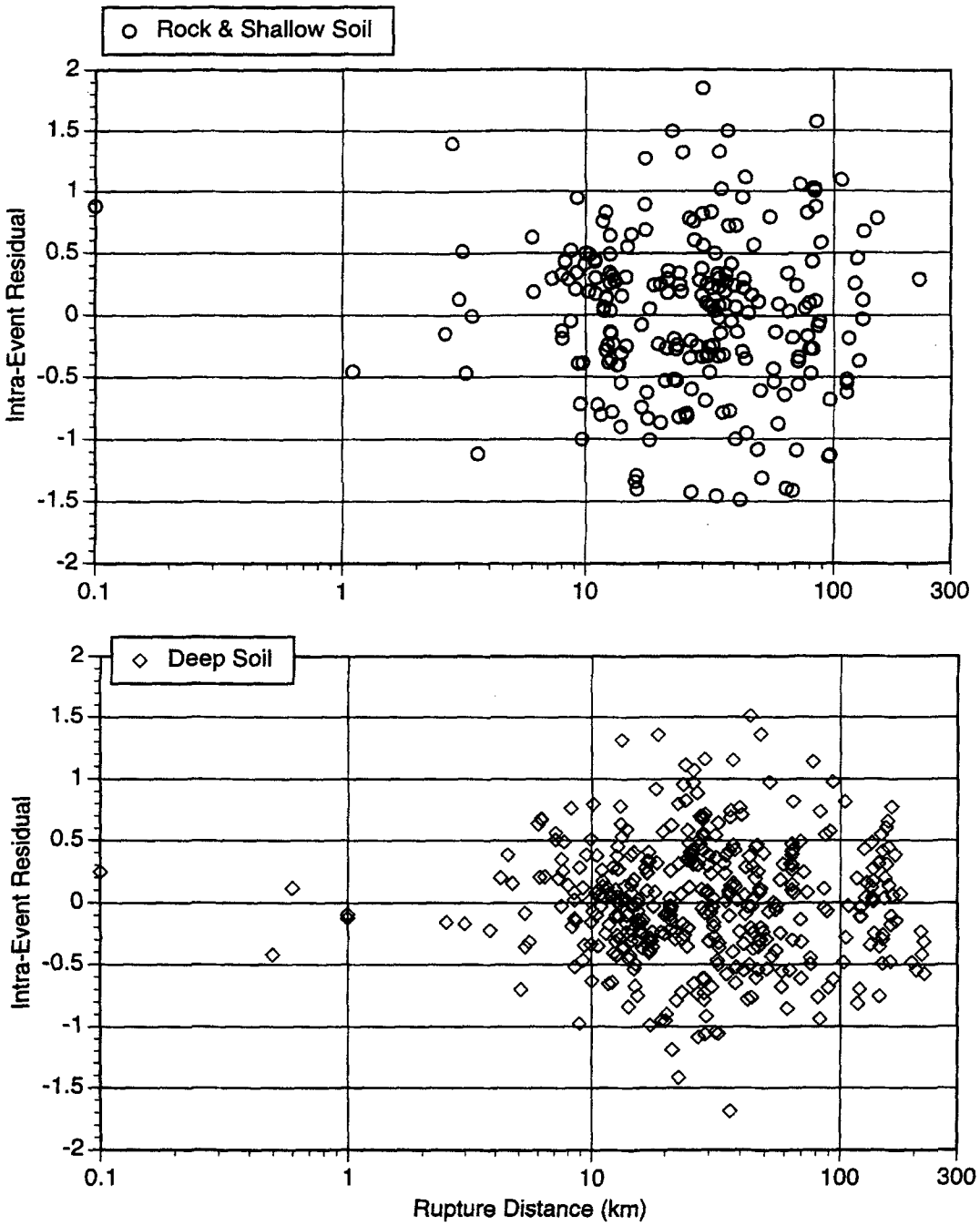

▲ **Figure 4a.** Distance dependence of the intra-event residuals for 1.0 second period for the horizontal component.

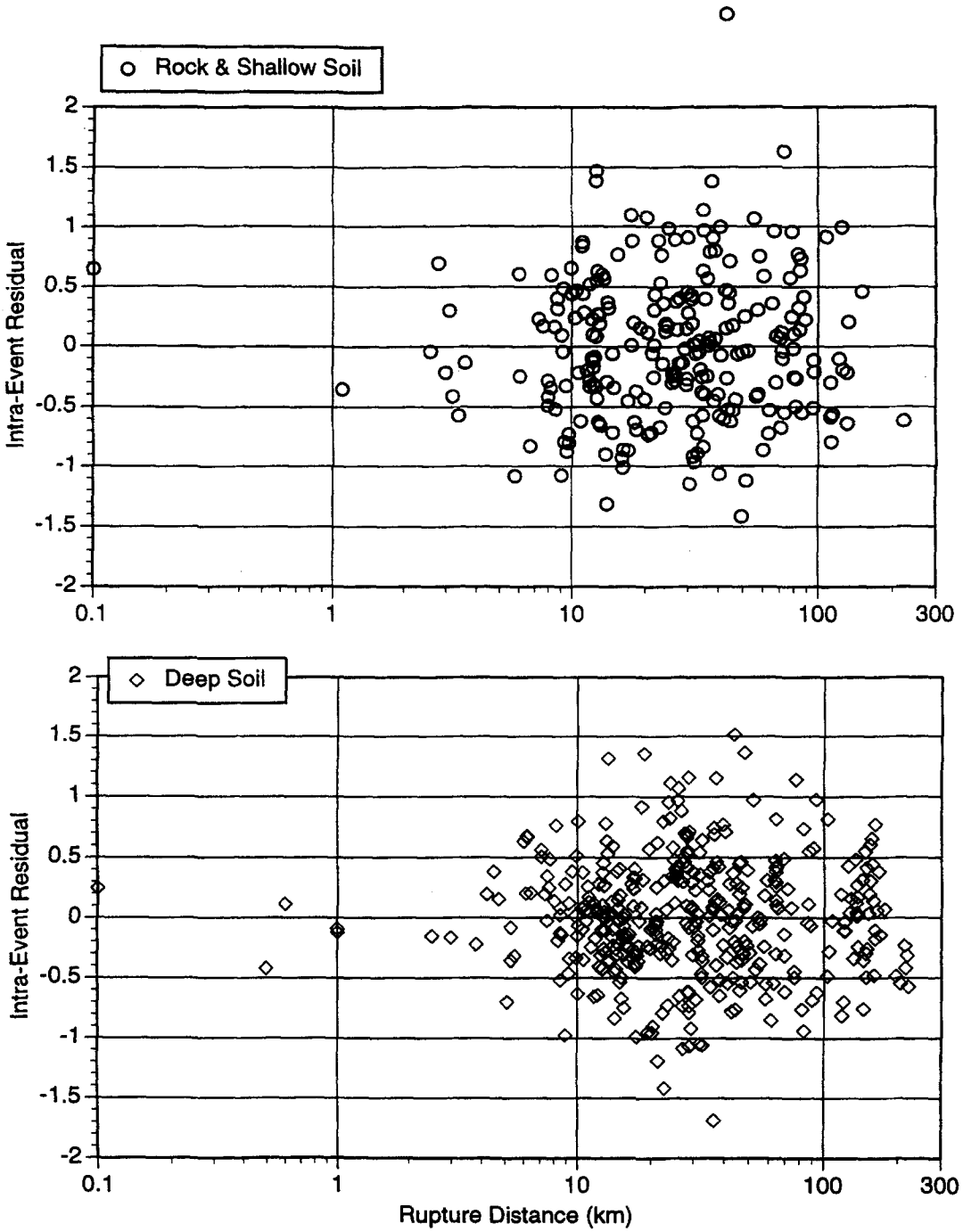

▲ **Figure 4b.** Distance dependence of the intra-event residuals for 0.3 second period for the horizontal component.

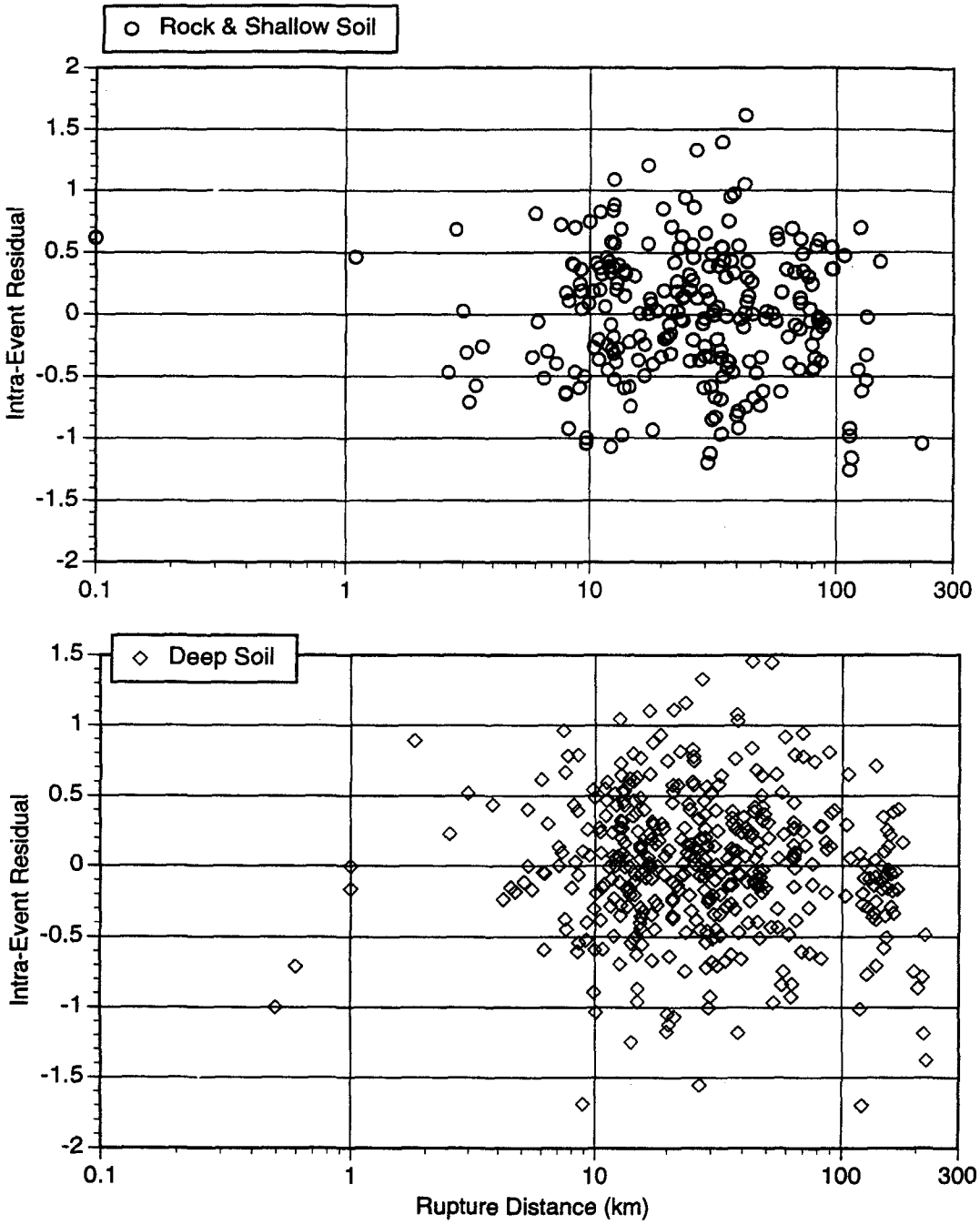

▲ **Figure 4c.** Distance dependence of the intra-event residuals for 0.1 second period for the horizontal component.

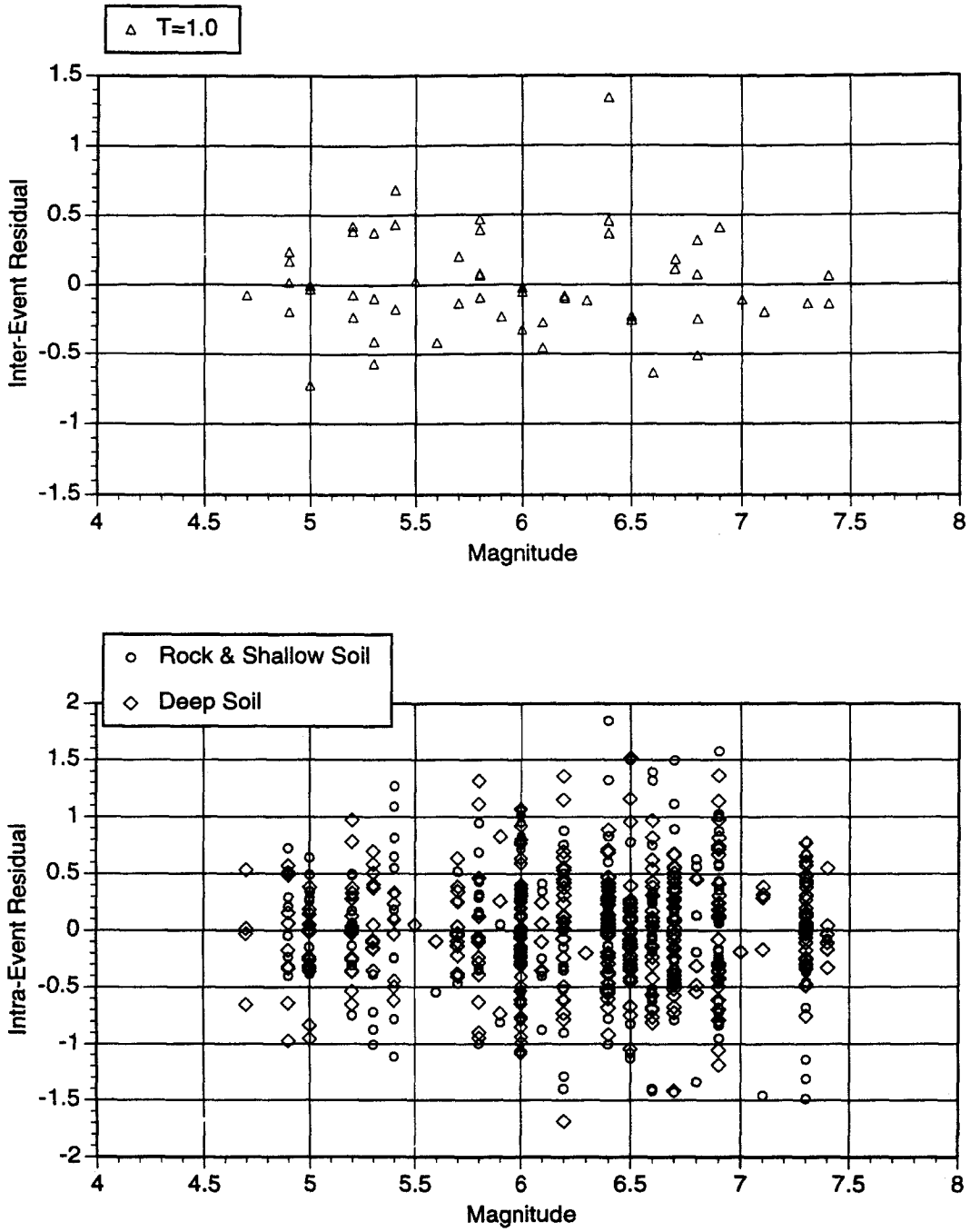

▲ **Figure 5a.** Magnitude dependence of the inter-event residuals (top) and the intra-event residuals (bottom) for 1.0 second period for the horizontal component.

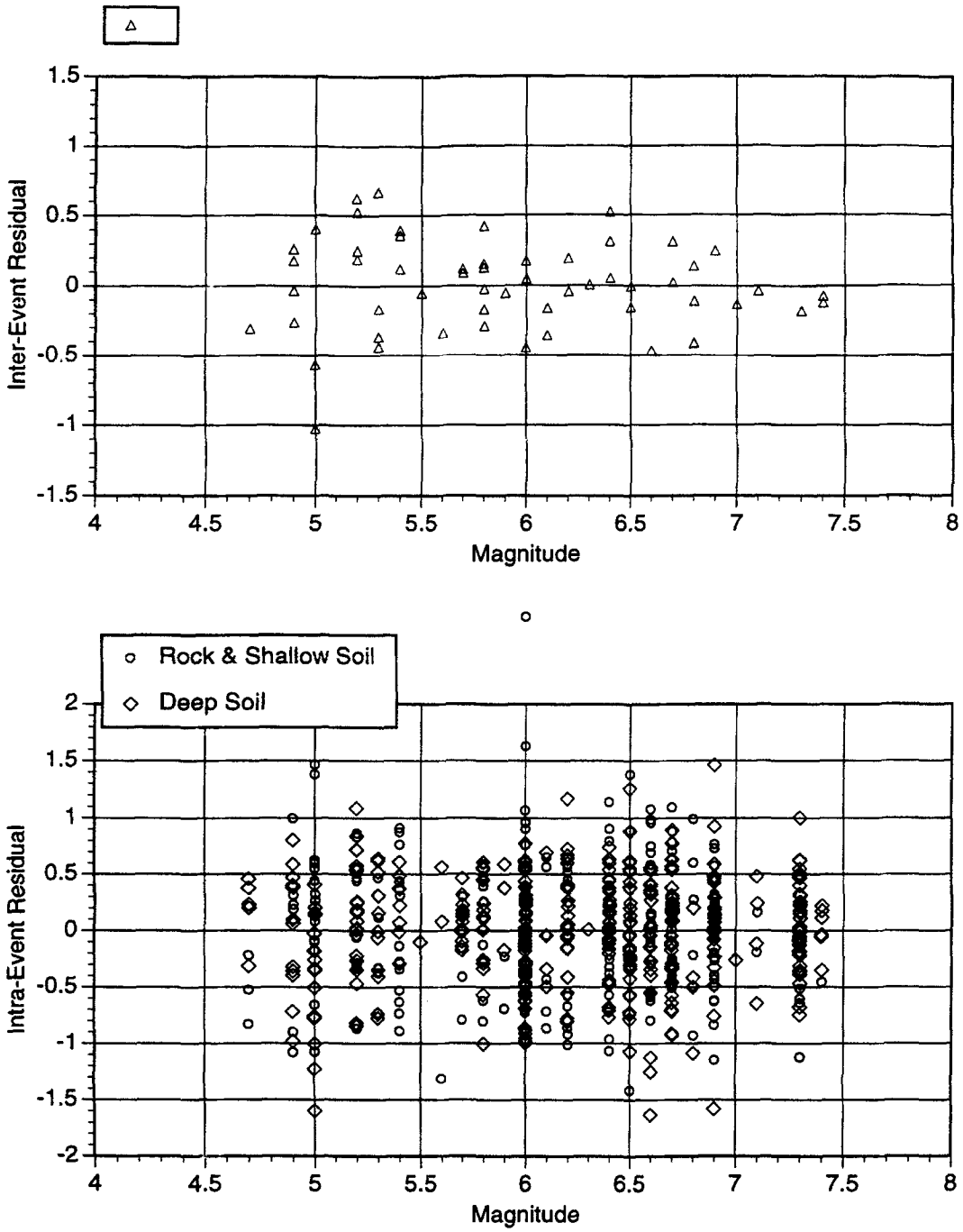

▲ **Figure 5b.** Magnitude dependence of the inter-event residuals (top) and the intra-event residuals (bottom) for 0.3 second period for the horizontal component.

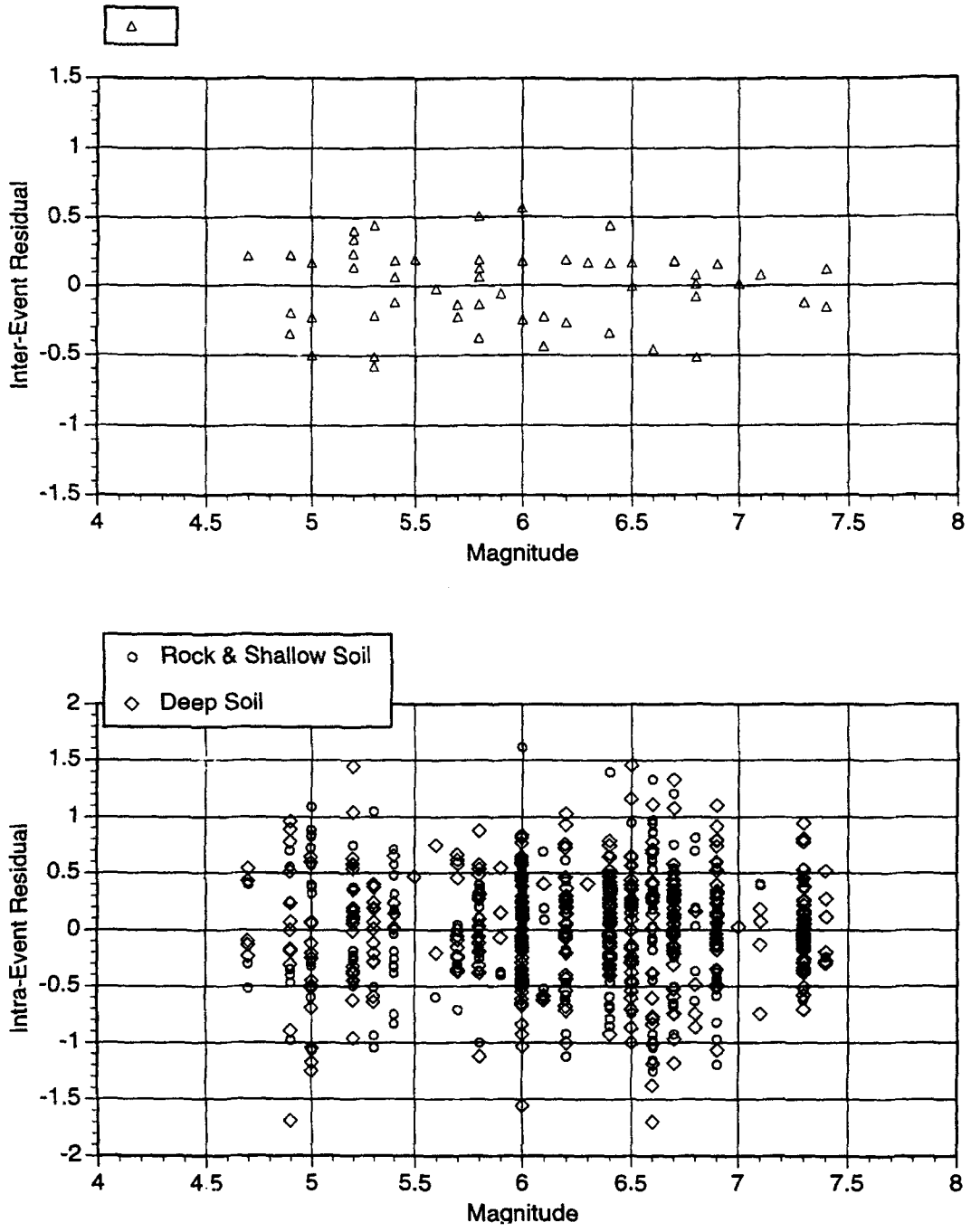

▲ **Figure 5c.** Magnitude dependence of the inter-event residuals (top) and the intra-event residuals (bottom) for 0.1 second period for the horizontal component.

TABLE 5.
Coefficients for the Vertical Component

Period	c_4	a_1	a_2	a_3	a_4	a_5	a_6	a_9	a_{10}	a_{11}	a_{12}	a_{13}	c_1	c_5	n
5.00	2.50	−2.053	0.909	−0.7200	0.275	0.260	−0.100	0.240	0.040	−0.220	−0.0670	0.06	6.4	0.3	3
4.00	2.50	−1.857	0.909	−0.7200	0.275	0.260	−0.100	0.240	0.040	−0.220	−0.0565	0.06	6.4	0.3	3
3.00	2.50	−1.581	0.909	−0.7200	0.275	0.260	−0.100	0.240	0.040	−0.220	−0.0431	0.06	6.4	0.3	3
2.00	2.50	−1.224	0.909	−0.7200	0.275	0.260	−0.008	0.240	0.040	−0.220	−0.0240	0.06	6.4	0.3	3
1.50	2.50	−0.966	0.909	−0.7285	0.275	0.260	0.058	0.240	0.025	−0.220	−0.0180	0.06	6.4	0.3	3
1.00	2.50	−0.602	0.909	−0.7404	0.275	0.260	0.150	0.240	0.004	−0.220	−0.0115	0.06	6.4	0.3	3
0.85	2.50	−0.469	0.909	−0.7451	0.275	0.309	0.150	0.273	−0.004	−0.220	−0.0097	0.06	6.4	0.3	3
0.75	2.50	−0.344	0.909	−0.7488	0.275	0.348	0.150	0.299	−0.010	−0.220	−0.0083	0.06	6.4	0.3	3
0.60	2.85	−0.087	0.909	−0.7896	0.275	0.416	0.150	0.345	−0.022	−0.220	−0.0068	0.06	6.4	0.3	3
0.50	3.26	0.145	0.909	−0.8291	0.275	0.471	0.150	0.383	−0.031	−0.220	−0.0060	0.06	6.4	0.3	3
0.46	3.45	0.271	0.909	−0.8472	0.275	0.497	0.150	0.400	−0.035	−0.220	−0.0056	0.06	6.4	0.3	3
0.40	3.77	0.478	0.909	−0.8776	0.275	0.539	0.150	0.428	−0.043	−0.220	−0.0050	0.06	6.4	0.3	3
0.36	4.01	0.617	0.909	−0.9004	0.275	0.571	0.150	0.450	−0.048	−0.220	−0.0047	0.06	6.4	0.3	3
0.30	4.42	0.878	0.909	−0.9400	0.275	0.580	0.150	0.488	−0.057	−0.220	−0.0042	0.06	6.4	0.3	3
0.24	4.93	1.312	0.909	−1.0274	0.275	0.580	0.109	0.533	−0.069	−0.220	−0.0035	0.06	6.4	0.3	3
0.20	5.35	1.648	0.909	−1.0987	0.275	0.580	0.076	0.571	−0.078	−0.220	−0.0030	0.06	6.4	0.3	3
0.17	5.72	1.960	0.909	−1.1623	0.275	0.580	0.047	0.604	−0.087	−0.220	−0.0025	0.06	6.4	0.3	3
0.15	6.00	2.170	0.909	−1.2113	0.275	0.580	0.024	0.630	−0.093	−0.220	−0.0022	0.06	6.4	0.3	3
0.12	6.00	2.480	0.909	−1.2986	0.275	0.580	−0.017	0.630	−0.104	−0.220	−0.0015	0.06	6.4	0.3	3
0.10	6.00	2.700	0.909	−1.3700	0.275	0.580	−0.050	0.630	−0.114	−0.220	−0.0010	0.06	6.4	0.3	3
0.09	6.00	2.730	0.909	−1.3700	0.275	0.567	−0.050	0.630	−0.119	−0.220	−0.0009	0.06	6.4	0.3	3
0.075	6.00	2.750	0.909	−1.3700	0.275	0.545	−0.050	0.630	−0.129	−0.220	−0.0007	0.06	6.4	0.3	3
0.06	6.00	2.710	0.909	−1.3700	0.275	0.518	−0.050	0.630	−0.140	−0.220	−0.0004	0.06	6.4	0.3	3
0.05	6.00	2.620	0.909	−1.3700	0.275	0.496	−0.050	0.630	−0.140	−0.220	−0.0002	0.06	6.4	0.3	3
0.04	6.00	2.420	0.909	−1.3700	0.275	0.469	−0.050	0.630	−0.140	−0.220	0.0000	0.06	6.4	0.3	3
0.03	6.00	2.100	0.909	−1.3168	0.275	0.432	−0.050	0.630	−0.140	−0.220	0.0000	0.06	6.4	0.3	3
0.02	6.00	1.642	0.909	−1.2520	0.275	0.390	−0.050	0.630	−0.140	−0.220	0.0000	0.06	6.4	0.3	3
0.01	6.00	1.642	0.909	−1.2520	0.275	0.390	−0.050	0.630	−0.140	−0.220	0.0000	0.06	6.4	0.3	3

TABLE 6.
Coefficients for Standard Errors for the Vertical Component

Period	b_5	b_6
5.00	0.78	0.050
4.00	0.75	0.050
3.00	0.72	0.050
2.00	0.69	0.050
1.50	0.69	0.050
1.00	0.69	0.050
0.85	0.69	0.050
0.75	0.69	0.050
0.60	0.69	0.050
0.50	0.69	0.050
0.46	0.69	0.050
0.40	0.69	0.050
0.36	0.69	0.050
0.30	0.69	0.050
0.24	0.69	0.050
0.20	0.69	0.050
0.17	0.70	0.056
0.15	0.72	0.063
0.12	0.74	0.075
0.10	0.76	0.085
0.09	0.76	0.085
0.075	0.76	0.085
0.06	0.76	0.085
0.05	0.76	0.085
0.04	0.76	0.085
0.03	0.76	0.085
0.02	0.76	0.085
0.01	0.76	0.085

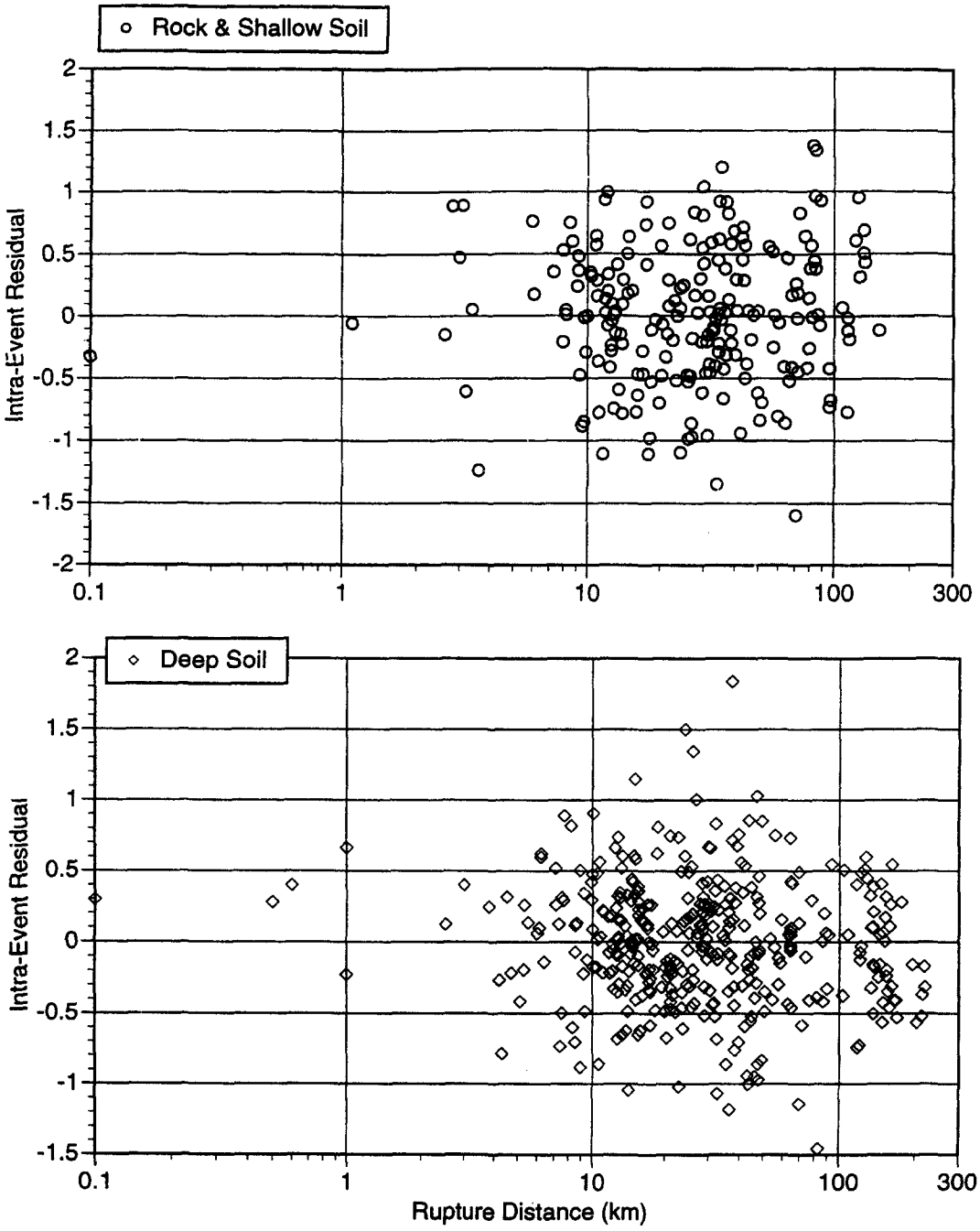

▲ **Figure 6a.** Distance dependence of the intra-event residuals for 1.0 second period for the vertical component.

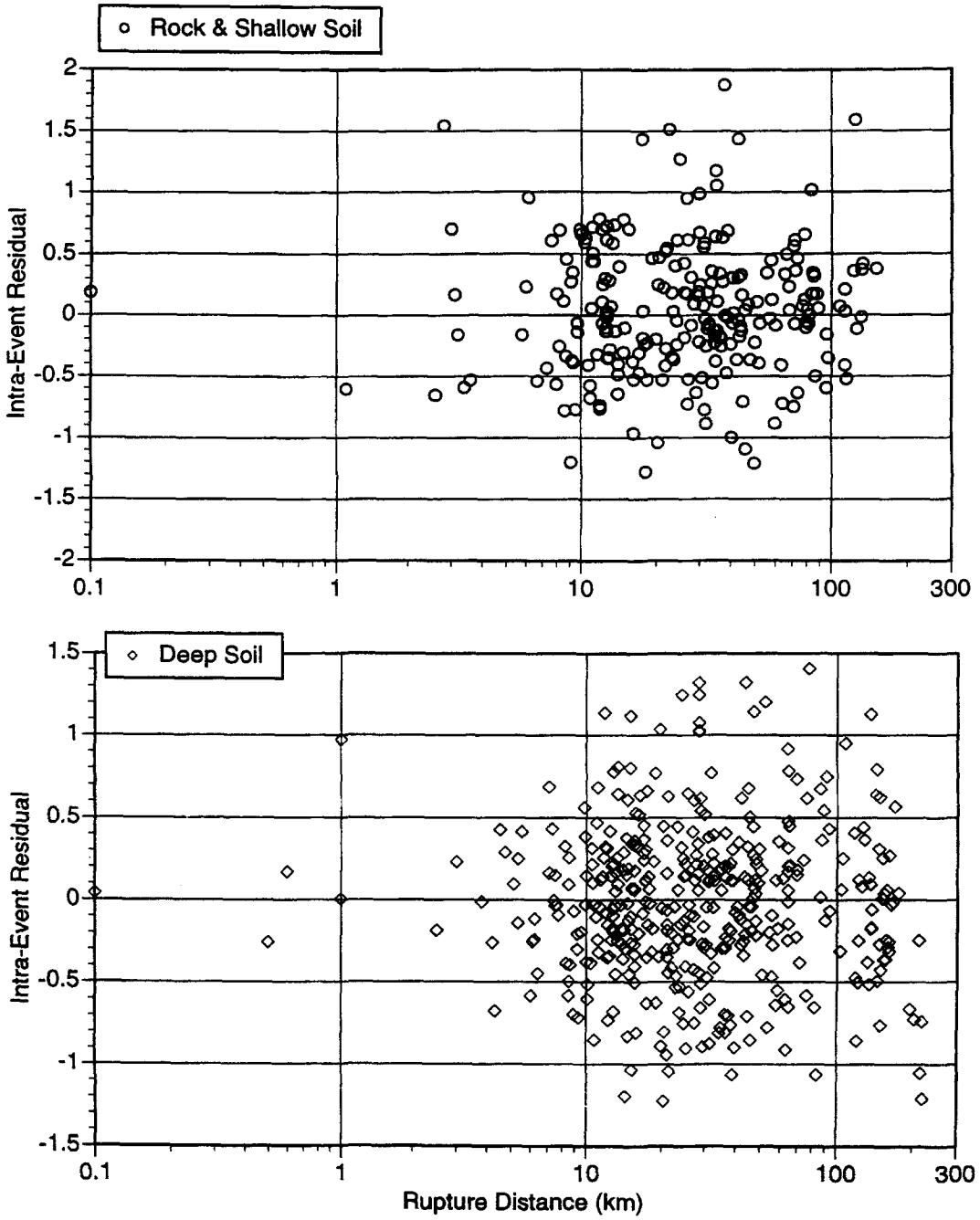

▲ **Figure 6b.** Distance dependence of the intra-event residuals for 0.3 second period for the vertical component.

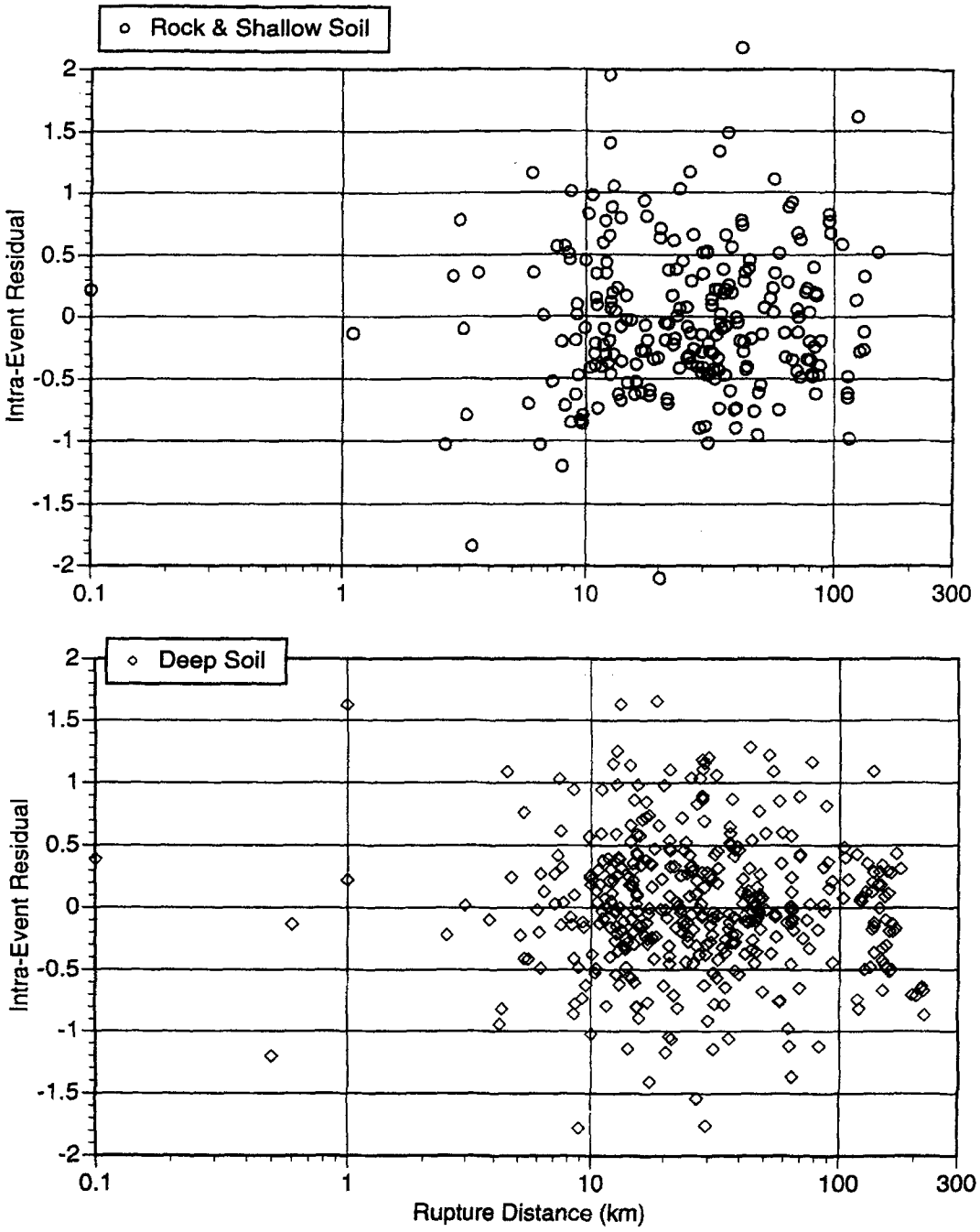

▲ **Figure 6c.** Distance dependence of the intra-event residuals for 0.1 second period for the vertical component.

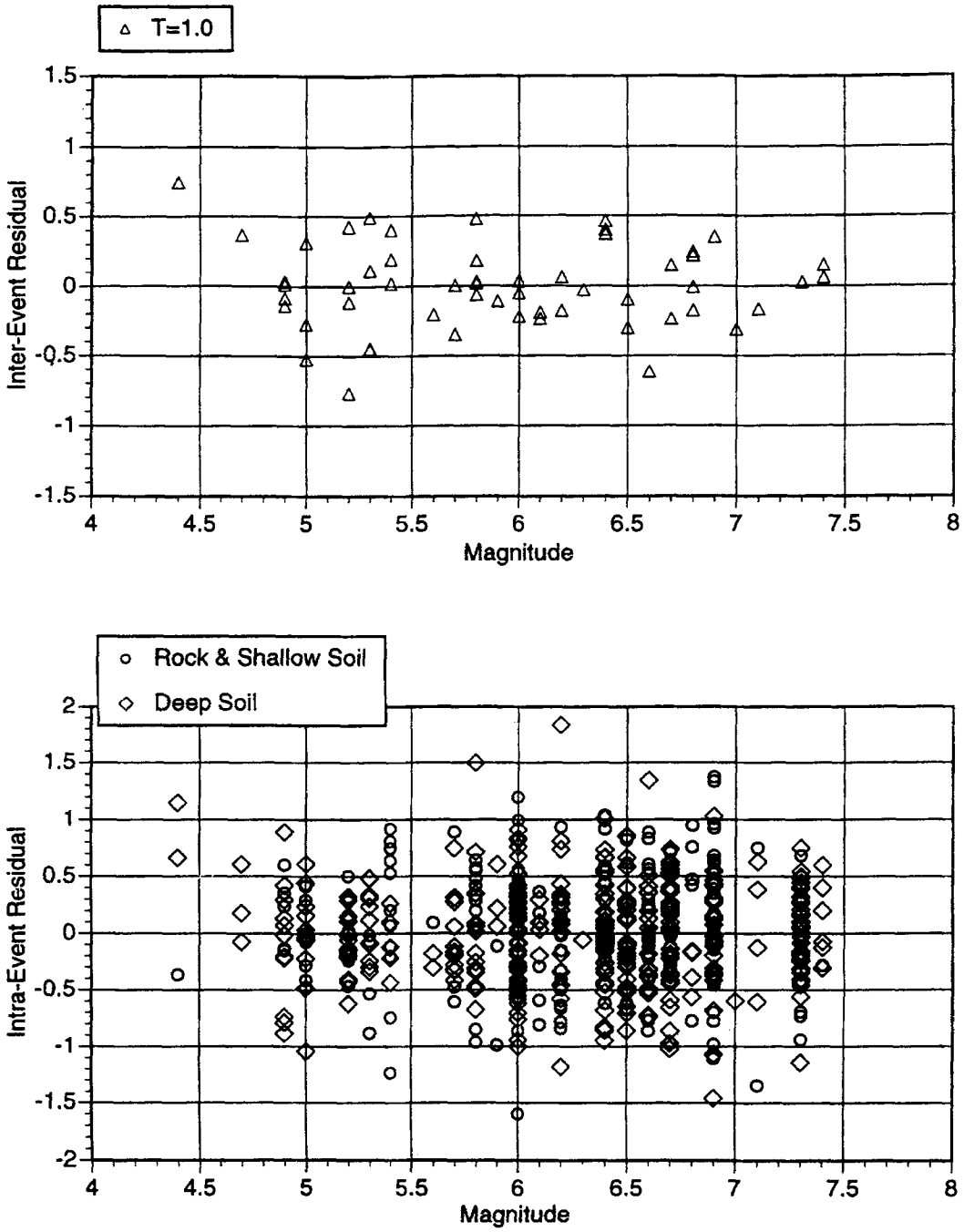

▲ **Figure 7a.** Magnitude dependence of the inter-event residuals (top) and the intra-event residuals (bottom) for 1.0 second period for the vertical component.

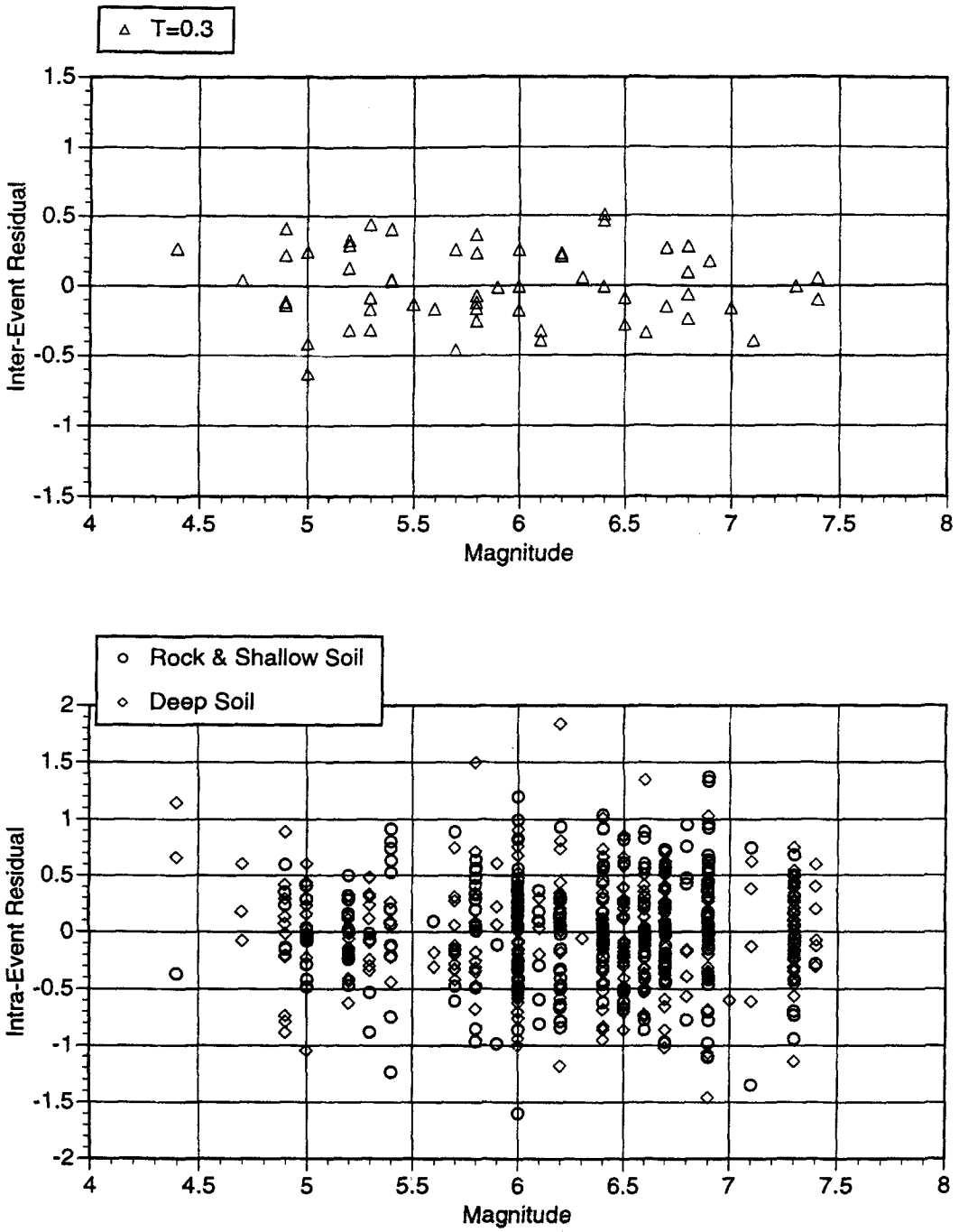

▲ **Figure 7b.** Magnitude dependence of the inter-event residuals (top) and the intra-event residuals (bottom) for 0.3 second period for the vertical component.

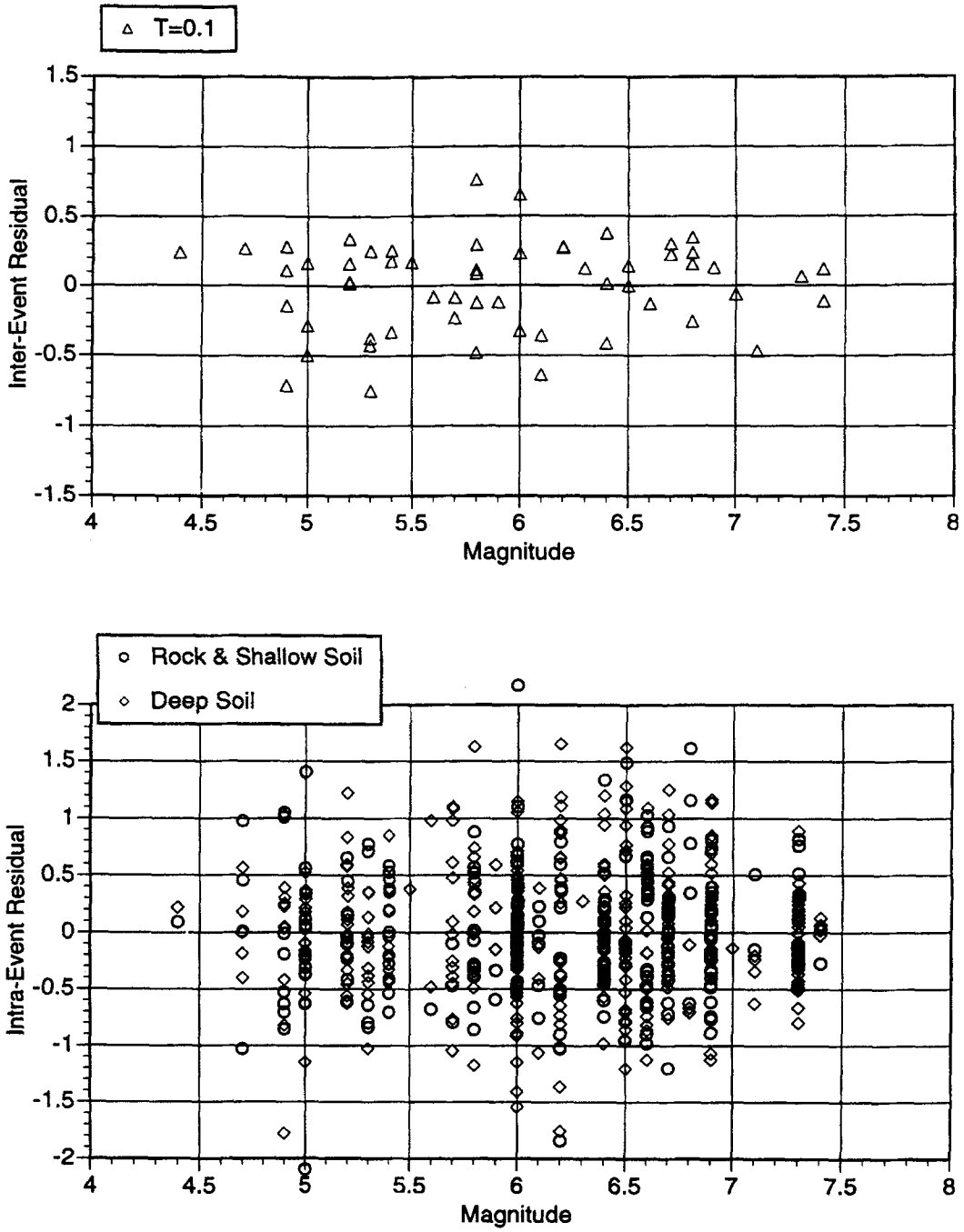

▲ **Figure 7c.** Magnitude dependence of the inter-event residuals (top) and the intra-event residuals (bottom) for 0.1 second period for the vertical component.

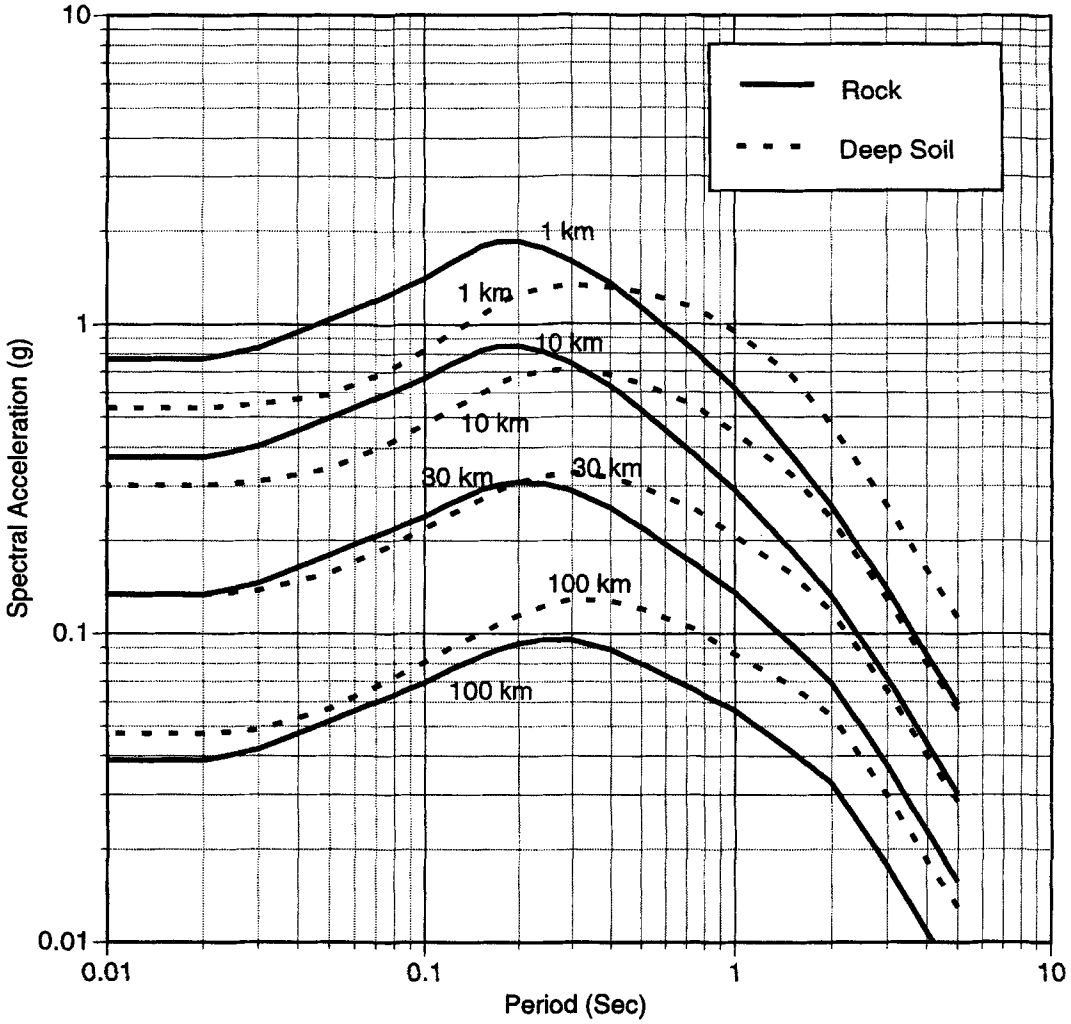

▲ **Figure 8.** Median model predictions for magnitude 7.0 strike-slip earthquakes for the average horizontal component.

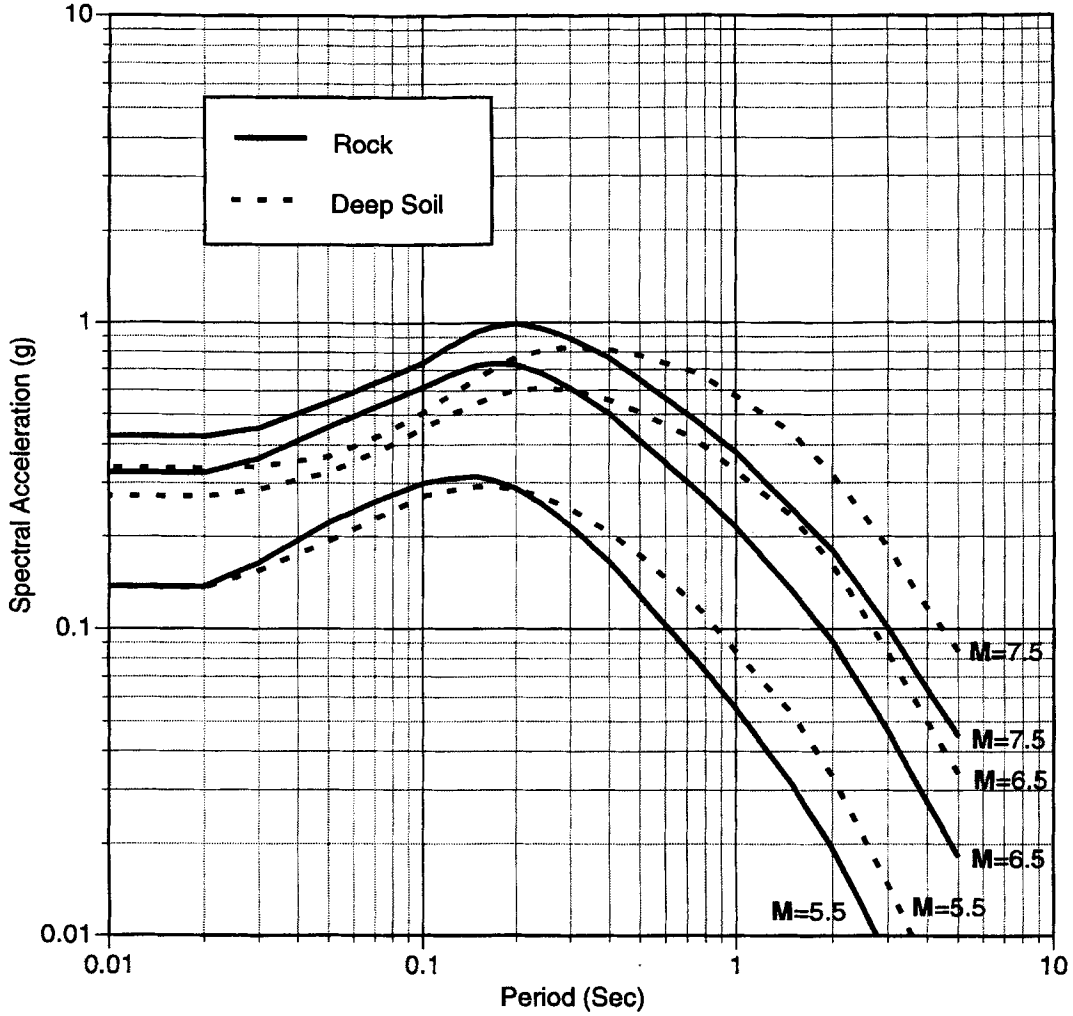

▲ **Figure 9.** Median model predictions for a strike-slip earthquake at a rupture distance of 10 km for the average horizontal component.

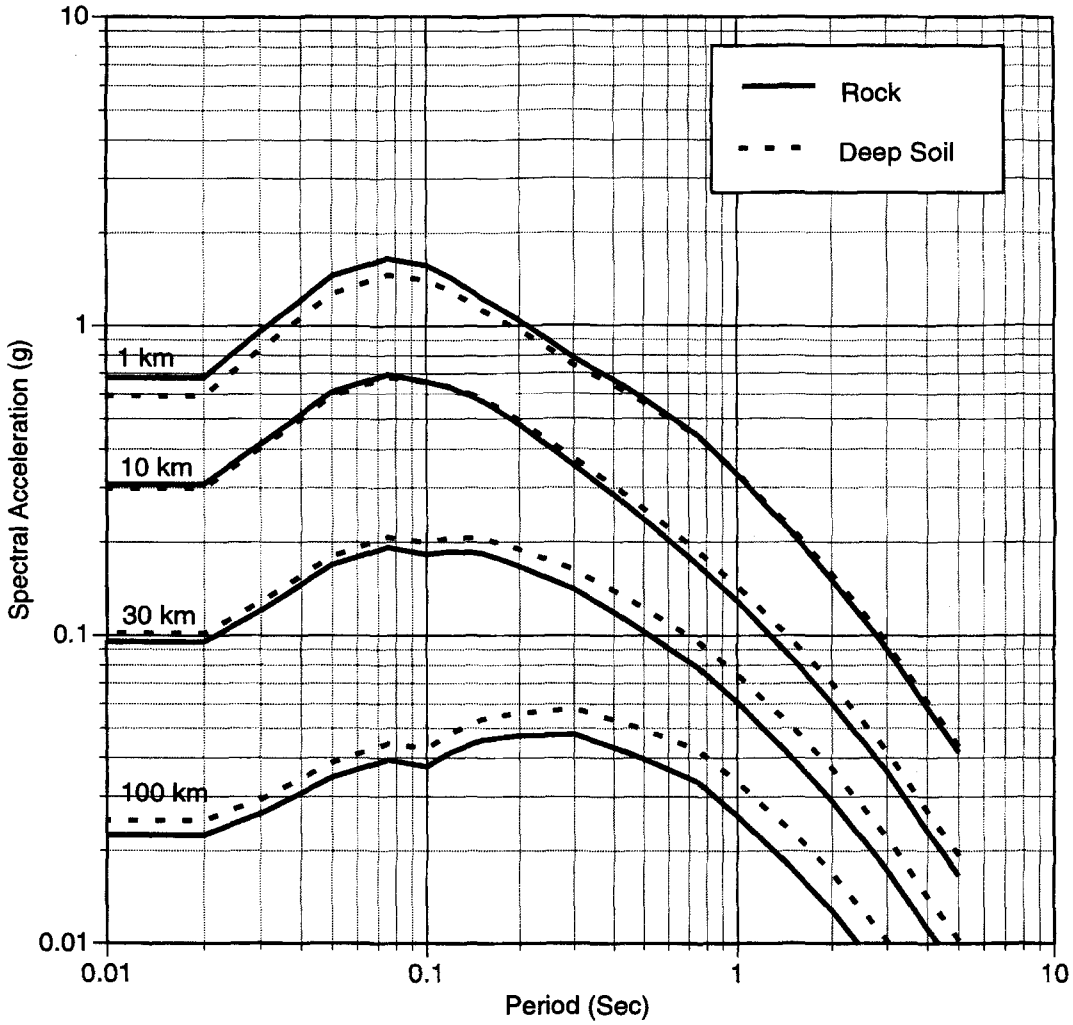

▲ **Figure 10.** Median model predictions for magnitude 7.0 strike-slip earthquakes for the vertical component.

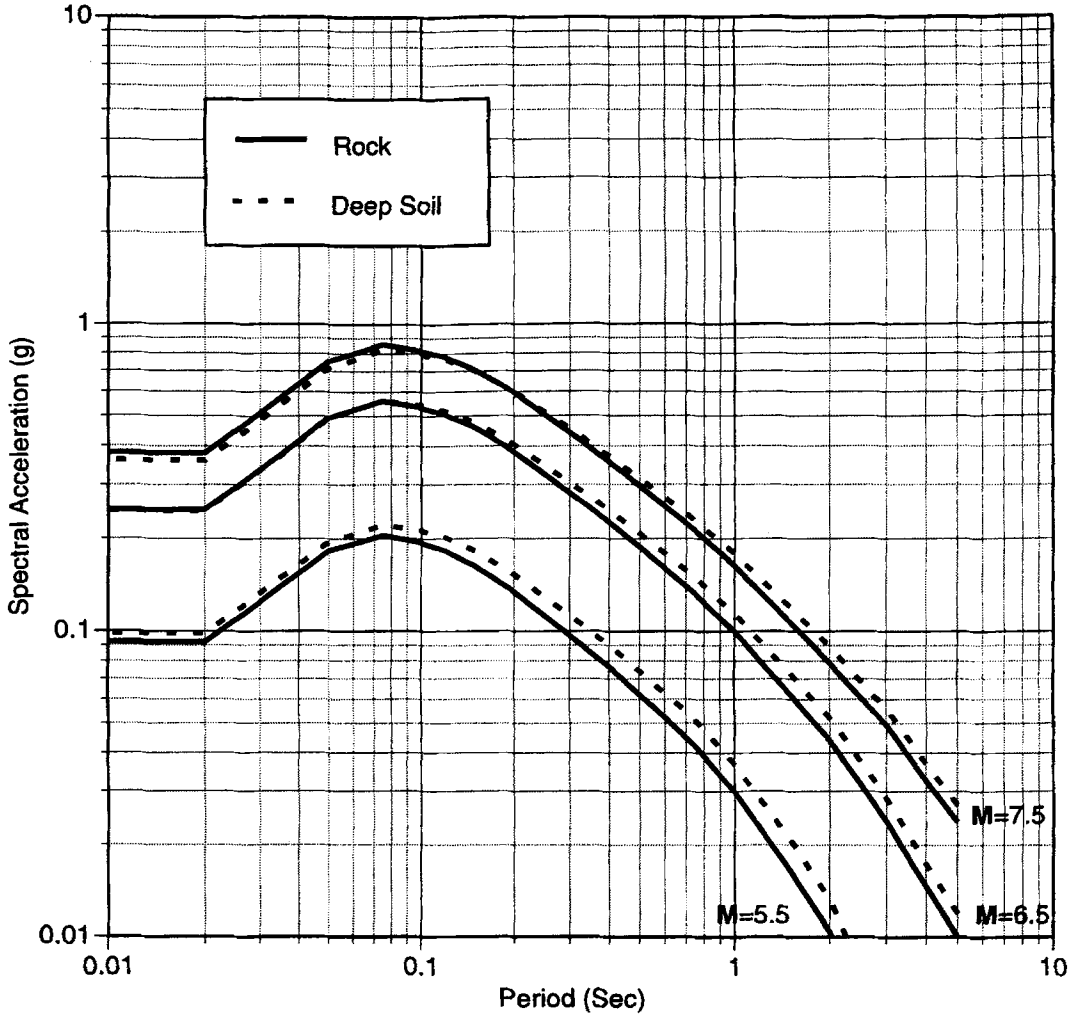

▲ **Figure 11.** Median model predictions for a strike-slip earthquake at a rupture distance of 10 km for the vertical component.